Investigations of Ash Layer Characteristics and Ash Distribution in a Diesel Particulate Filter using Novel Lubricant Additive Tracers

by

Ryan Morrow

Submitted to the Department of Mechanical Engineering in Partial Fulfillment of the Requirements for the Degree of

BACHELORS OF SCIENCE IN MECHANICAL ENGINEERING

AT THE

MASSACHUSETTS INSTITUTE OF TECHNOLOGY

[June 2010]
May 2010

Signature of Author. _____
Department of Mechanical Engineering
May 10, 2010

Certified by: _____
Alexander Sappok
Postdoctoral Associate
Thesis Supervisor

Certified by: _____
Victor W. Wong
Principal Research Scientist and Lecturer in Mechanical Engineering

Accepted by: _____
John H. Lienhard V
of Mechanical Engineering
Chairman, Undergraduate Thesis Committee

(This page intentionally left blank)

Investigations of Ash Layer Characteristics and Ash Distribution in a Diesel Particulate Filter using Novel Lubricant Additive Tracers

by

Ryan Morrow

Submitted to the Department of Mechanical Engineering on May 10, 2010 in Partial Fulfillment of the Requirements for the Degree of

BACHELORS OF SCIENCE IN MECHANICAL ENGINEERING

ABSTRACT

Diesel particulate filters (DPF) are currently widely used in various applications as a means of collecting particulate matter in order to meet increasingly stringent particle emissions regulations. Over time, the DPF slowly accumulates incombustible material or ash, mostly from the metallic additives present in the engine lubricant. This build up of accumulated ash leads to an increase in flow restriction and therefore an increase in pressure drop along the DPF. The increased pressure drop negatively impacts engine performance and fuel economy, and it also requires eventual filter removal for ash cleaning.

While the major effects of ash accumulation on DPF performance are known, the fundamental underlying mechanisms are not. This work is focused on understanding key mechanisms, such as the soot deposition and the ash formation, accumulation, and distribution processes, which play a major role in determining the magnitude of the ash effect on DPF pressure drop. More specifically, it explores the location of ash deposit accumulation inside the DPF channels, whether in a layer along the filter walls or packed in a plug at the rear of the channels, which is one of the key factors controlling DPF pressure drop. A specialized experiment was set up by running three different lubricants, each with its own unique additive tracer, sequentially through a diesel burner system. Scanning electron microscopy (SEM) was used to analyze the evolution of the ash deposits in the DPF samples in order to explain the specific mechanisms and processes controlling ash properties and their effect on DPF pressure drop.

The experimental results were compared and correlated with previous DPF test data and theoretical models, providing additional insight to optimize diesel particulate filter performance. The results are useful in optimizing the design of the engine, aftertreatment, and lubricant systems for future diesel engines, balancing the requirements of additives for adequate engine protection with the requirements for robust aftertreatment systems.

Thesis Supervisor: Alexander Sappok
Title: Postdoctoral Associate in Mechanical Engineering

(This page intentionally left blank)

ACKNOWLEDGEMENTS

Alex Sappok

Victor Wong

Patrick Boisvert

Yinlin Xie

(This page intentionally left blank)

TABLE OF CONTENTS

LIST OF FIGURES

LIST OF TABLES

NOMENCLATURE

Ca	Calcium
DPF	Diesel Particulate Filter
EDX	Energy Dispersive X-ray Spectrometry
Mg	Magnesium
P	Phosphorous
PM	Particulate Matter
S	Sulfur
SEM	Scanning Electron Microscope
Zn	Zinc

1 OBJECTIVES AND BACKGROUND

As ash accumulates in the diesel particulate filter (DPF), the backpressure in the filter increases and ultimately results in a reduction in fuel economy. This ash build-up limits the useful life of the DPF and requires periodic cleaning of the filter. Overall, the ash distribution inside of the filter has proven to be a very important factor affecting DPF performance.

The deleterious effect of ash on DPF performance creates the need to analyze the distribution of ash particles in the DPF. This study aims to understand the ash deposit and layer formation along the DPF channel walls through a detailed analysis of the key factors, such as shear stress, governing ash transport.

1.1 Diesel Particulate Filter

Diesel particulate filters are generally ceramic filters used in diesel engines to reduce particle emissions. In order to do so, it utilizes a wall-flow substrate design and combines surface-type and deep-bed filtration mechanisms. Diesel particulate matter consists of carbon, condensed hydrocarbons, sulfates and ash. Either continuous or periodic thermal regeneration is utilized to remove the collected particulate matter in the DPF. However, ash from lubricant additives remains in the channel and builds up over time. The DPFs have been used in certain "retrofit applications" since the 1980's and currently are outfitted on all 2007 and newer on-road engines in the United States. [1]

1.2 Ash Properties and Characteristics

It is useful to first understand key ash properties and parameters before describing the detailed mechanisms. Ash is initially deposited within the soot layer along the DPF channel walls. Following regeneration, ash may be carried to the back of the DPF when the shear stress present in the DPF channel is greater than the ash's critical shear stress, or the shear stress required to separate the ash. The ash "stickiness" depends on the

filter's temperature history, the ash composition, and also the critical ash "sticking" temperature. As exhaust flows through the channel, the "sticky" ash will deposit along the walls while the "non-sticky" ash is transported towards the end of the filter to the plug. [2]

The ash can also alter the geometry of the DPF channel. As ash builds up on the DPF channel wall, the inlet of the channel contracts. This creates a smaller flow cross section, which can lead to higher velocities in the channel and therefore a higher channel shear stress. The ash plug formed in the back of the channel also reduces the effective length of the filter. The plug size is dependent on ash density and the amount of ash accumulated, and leads to an overall pressure drop along the filter length. [3]

Understanding these properties, one can see that there are essentially two ways to mitigate ash effect: either make less ash, or control its properties when packed in the back of the filter.

1.2.1 Ash Accumulation

Lubricant ash generally deposits in a layer along the channel walls and in plugs at the back in the DPF. Currently, a significant amount of work has been focused on understanding, from a theoretical perspective, the governing processes. Figure 1.1 shows the ash accumulation processes and the ash plug formation.

Following the diesel engine's combustion cycle, particulate matter, metal debris, liquid sulfates, lubricant ash (ie. Ca, Mg, Zn, S, and P), and sulfur dioxide are carried in the exhaust and into the DPF. First, the particulate matter (PM) and ash are evenly distributed along the DPF channel wall, while the sulfur dioxide passes through the filter wall and exits the filter. Over time, PM and ash accumulate on the channel walls before PM oxidation and ash agglomeration / sintering takes place. Next, some of the ash may be transported to the back of the DPF, and after repeated regenerations, an ash layer remains along the wall while an ash plug forms and grows from the end of the channel.

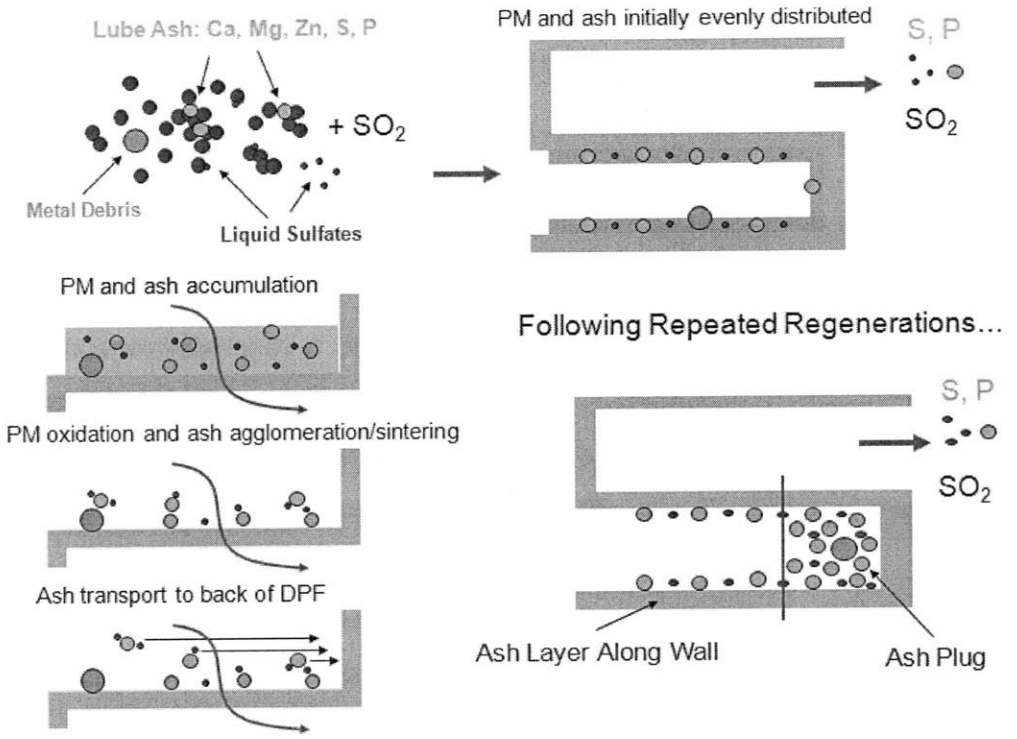

Figure 1.1. Ash accumulation and plug formation process. [4]

1.2.2 Ash Distribution over Time

The distribution of the accumulated ash in the DPF changes with time. Figure 1.2 demonstrates the distribution of the ash in the overall channel.

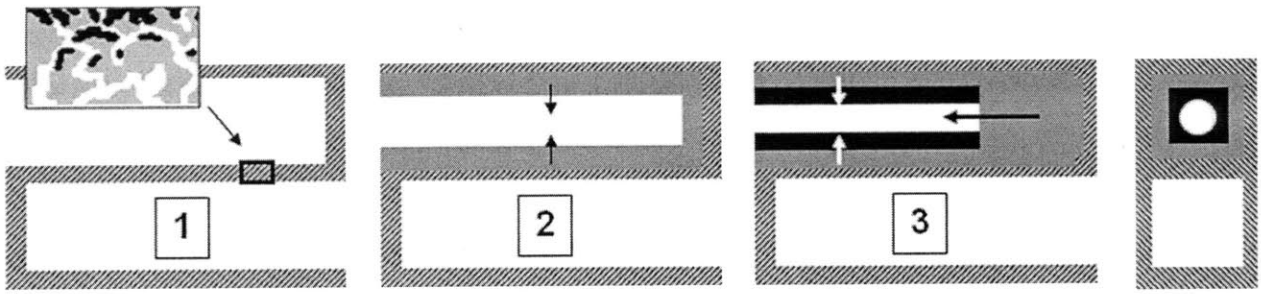

Figure 1.2. Ash distribution in channel over time. [4]

As ash first accumulates in a clean DPF, it initially covers the surface pores of the filter. Then, layers of ash begin to build up on the channel wall and thicken. Once the layers reach a certain critical thickness, the ash is sheared off and transported to the back of the channel, and a plug begins to form in the channel. The ash typically forms a small, restrictive circular profile in the channel. Figure 1.3 shows a closer look at how the ash layer forms on the channel wall.

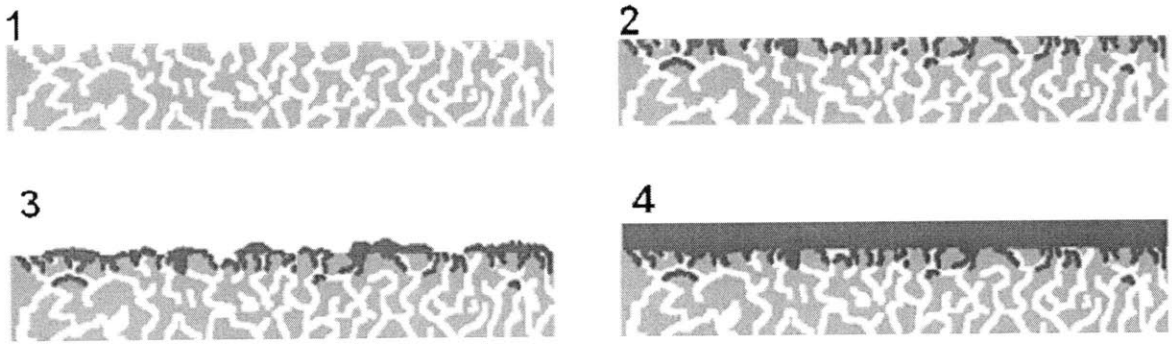

Figure 1.3. Formation of ash layer on DPF channel wall. [4]

Looking closely at the clean DPF wall, ash first fills the surface pores of the DPF, Figure 1.3, step #2. Next ash begins to accumulate above the pores in the wall, Figure 1.3, step #3. Eventually, a layer of ash begins to form above the filter surface and grows as the ash accumulates, shown in step #4 of Figure 1.3.

1.2.3 Ash Properties

In order to investigate the ash characteristics, certain key parameters affecting the ash properties need to be understood. First of all, ash is carried to the back of the channel and into the plug when the shear stress caused by the flow through the channel is greater than the critical shear stress of the ash (the shear stress required to separate the ash particles). The ash "stickiness" depends on both the DPF's temperature history, ash composition, and the critical ash "sticking" temperature, or the temperature required to cause the ash to stick to itself. When entering the DPF, the "sticky" ash deposits along the walls while the

"non-sticky" ash is more likely to be transported towards the end of the filter. As the ash layers build on the walls, the inlet of the channel contracts, creating a smaller flow cross section over time and affecting the flow speed and shear stress. Once a plug is created and begins to form, it reduces the effective length of the filter channel and leads to an overall pressure drop along the filter length. Additionally, the plug size is a function of ash density and the total amount of ash accumulated in the channel.

1.3 Theoretical Model

The influence of key parameters can be investigated using existing models developed at The Sloan Automotive Laboratory in order to simulate a DPF under various conditions. Figure 1.4 demonstrates the manner in which ash distribution affects pressure drop.

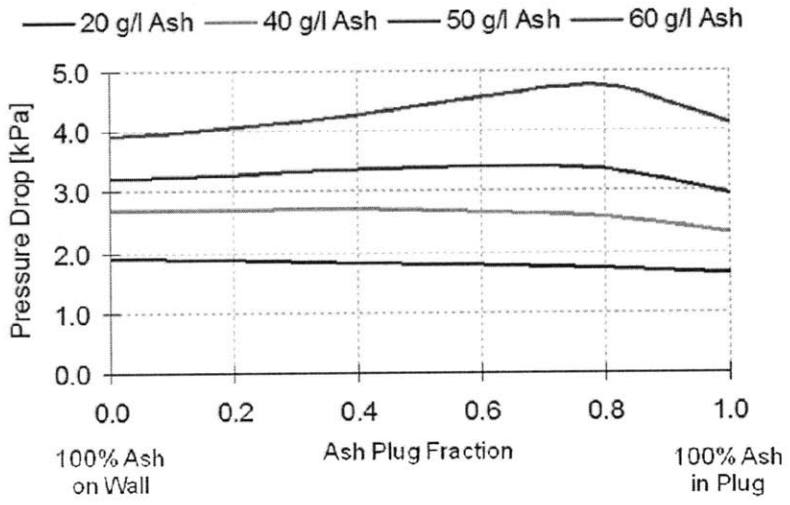

Figure 1.4. Effect of ash distribution of DPF pressure drop. [4]

The figure relates the simulated pressure drop with a DPF for different amounts of ash loading, as a function of ash distribution in the channel. An ash plug fraction of "0" corresponds to all ash in the channel being located on the wall and an ash plug fraction of "1" corresponds to all ash in the channel being located in the plug. The figure shows that at typical DPF ash levels (less than 40 grams/liter), packing all ash into the plug can actually reduce the pressure drop in the filter. However, a small amount of ash on the wall (about 20%) reduces the benefit of the ash-plug deposition. Additionally, for ash loads greater than 50 grams/liter, the plug will increase filter wall velocities significantly.

However, in reality soot also accumulates on the filter and needs to be accounted for. Figure 1.5 shows the same distribution but includes soot along with the ash.

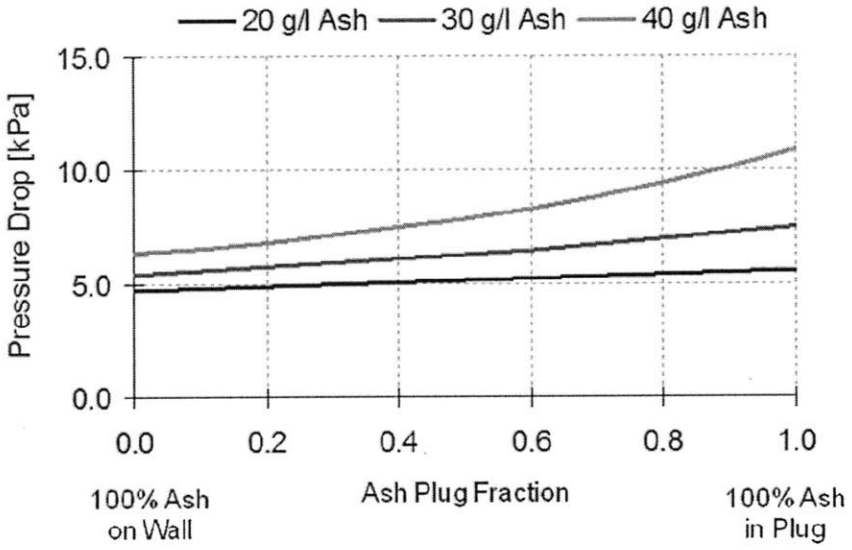

Figure 1.5. Effect of ash and soot distribution on DPF pressure drop – ash with 6 g/l soot. [4]

The figure shows DPF pressure drop as a function of ash distribution ranging from 100% on the channel wall to 100% of the ash in the plug, for three different amounts of ash loading. Additionally, the figure takes into consideration soot present on the ash layers. Accordingly for both ash and soot accumulated in the DPF, the lowest pressure drop is achieved by depositing all of the ash along the channel walls. The ash accumulated in the end-plug increases the wall velocities through the soot layer, which is approximately ten times less permeable than the ash layer.

Pressure drop is a direct function of ash layer thickness, which can in turn be influenced by the regeneration process. Figure 1.6 compares the ash layer thickness of continuous and periodic regeneration.

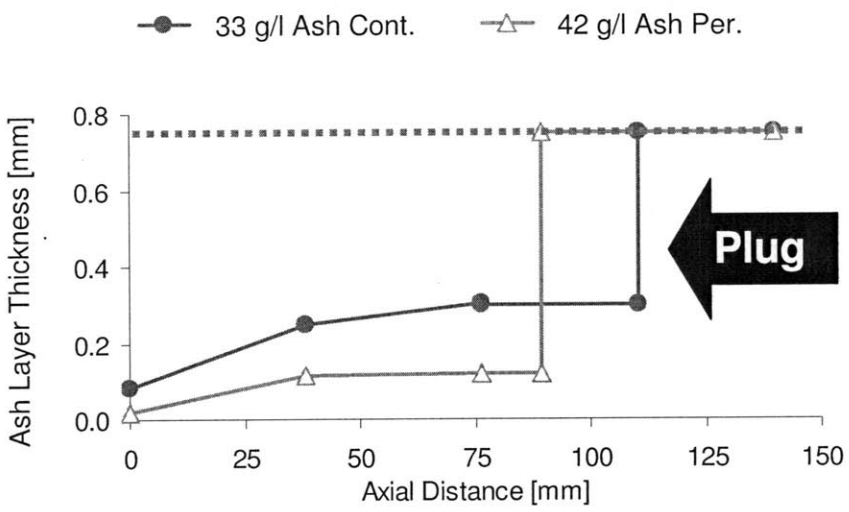

Figure 1.6. Ash layer thickness along DPF channel – Continuous versus periodic regeneration. [4]

From the figure, one can see that continuous regeneration generally leads to a thicker layer of ash along the DPF channel walls. Additionally, the plug does not develop until further down the channel. Figure 1.7 provides additional experimental data showing the effects of variations in ash distribution, from continuous and periodic regeneration, on DPF pressure drop.

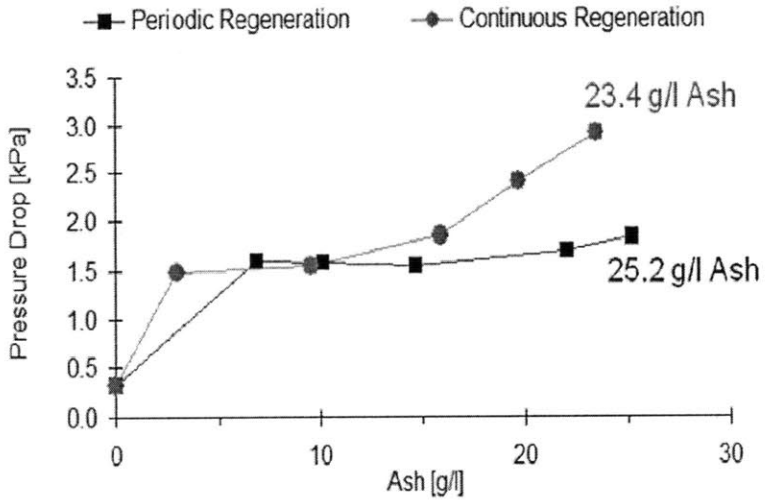

Figure 1.7. DPF pressure drop for continuous and periodic regeneration using a flow bench at 25°C, space velocity: 20,000 hr.

The figure clearly shows the location of ash deposits affects the filter pressure drop differently. Continuous regeneration leads to a thicker ash layer along the walls, imposing additional restrictions on the exhaust flow, thereby resulting in elevated pressure drop across the DPF.

All of this background information can be used in order to understand the theoretical framework. The experimental data and models clearly show a large effect of ash distribution on pressure drop. Given this background information, this work investigates several key objectives: studying the ash layer and quantifying the layer thickness, investigating ash plug formation and evolution, and understanding and proposing specific mechanisms controlling ash transport.

2 TEST SETUP AND PROCEDURES

The following section presents the experimental setup and procedure, used to study the ash layers and plugs in the DPF.

2.1 KEY TEST PARAMETERS AND PROCEDURE

In order to carry out the analysis, a DPF was first loaded with ash. A catalyzed cordierite DPF, measuring 5.66" in diameter and 6" in length was used. Three separate lubricant additive tracers were used, in sequence, to track the ash layer formation. Each lubricant was formulated to 1% sulfated ash and consumed in a custom accelerated ash loading system in series, at 7 kg of each oil. The exposure sequence was Ca, followed by Zn, and then finally Mg. Table 2.1 displays the elemental composition of each lubricant tracer as a percentage of weight.

Elemental Composition [wt. %]			
	Base + Ca	**Base + Mg**	**Base + Zn**
Zn			0.358
P			0.328
Ca	0.295		
Mg		0.207	
S	0.035	0.046	0.686
Total	**0.33**	**0.253**	**1.372**

Table 2.1. Elemental composition of each lubricant additive tracers.

Each of the three tracers had one of the following main elements: calcium, magnesium, and zinc. Sulfur is also present in each of the tracers, although the amount in the zinc-based lubricant is much higher than any of the other lubricants. Additionally, the zinc-based lubricant also contains a large amount of phosphorus. Use of these elements as

tracers allows for analysis of the ash layer formation and build-up processes following the test, as the time history and sequence of the specific oils is known.

For the test procedure, the target DPF ash loading level was 10 grams/liter with each of the previously mentioned lubricant tracers in order (Ca, Zn, Mg). During the test, the DPF pressure drop was also measured at different intervals. Further, the DPF was also loaded with soot to 3-4 g/L, using a Cummins ISB engine. Once again, the DPF pressure drop was measured at the target ash/PM load. After each of these sequences were carried out, a detailed DPF post-mortem analysis was conducted.

2.2 DPF PERFORMANCE EVALUATION

Before looking into the post-mortem analysis, it is useful to understand the manner in which the ash build-up affects DPF performance. First, the amount of ash created in each stage / by each lubricant was recorded, as demonstrated by Figure 2.1.

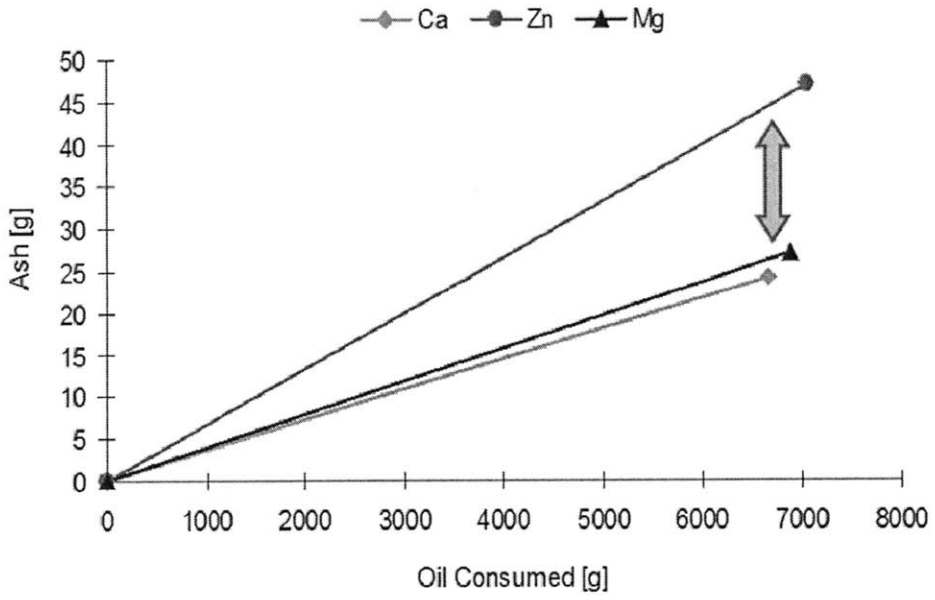

Figure 2.1. DPF ash accumulation and variation with the different lubricants.

Equal amounts of lubricant were consumed for each test (7 kg). However, nearly twice as much ash was produced with the base oil that contained Zn as compared to the oils formulated with Mg and Ca. These increased ash levels are attributed to the formation of zinc phosphates and sulfates, as this oil contained significantly higher P and S levels, shown in Table 2.1. Additionally, the pressure drop was recorded and is displayed in Figure 2.2.

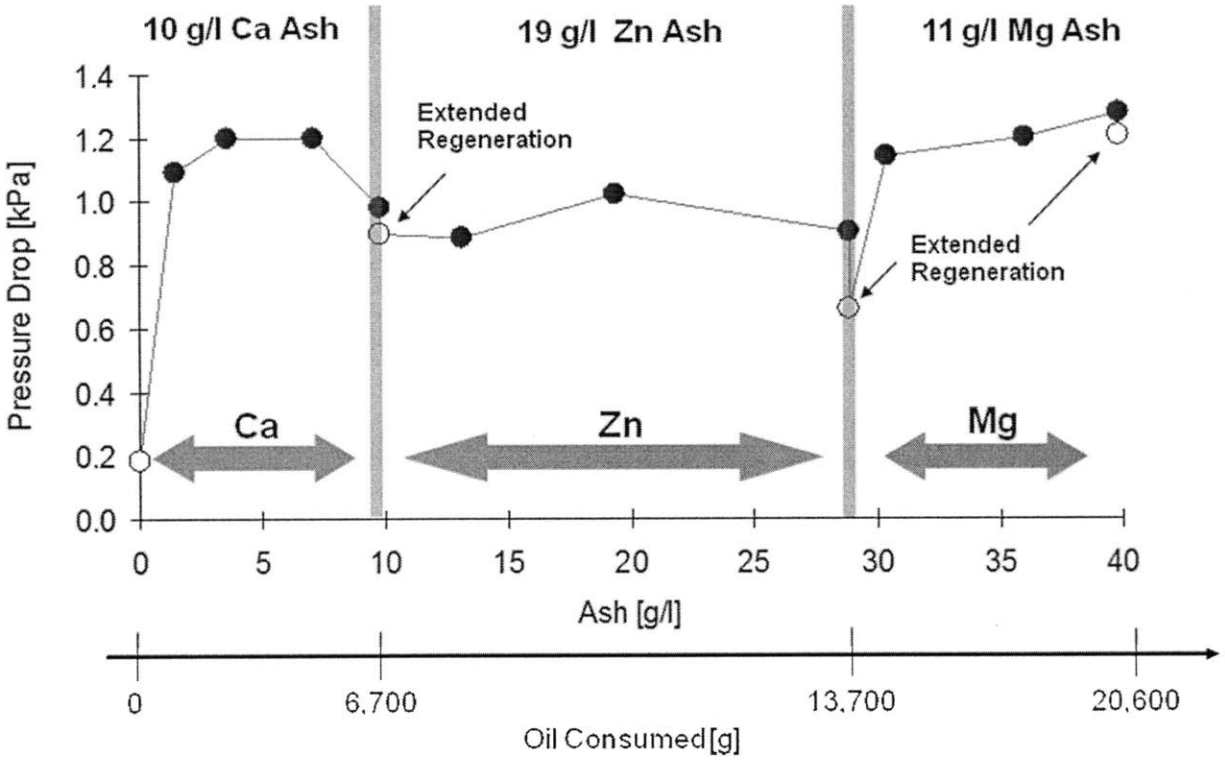

Figure 2.2. DPF pressure drop evolution with additive tracers.

The pressure drop trends presented in figure 2.2 is only due to ash accumulation in the DPF. Ca and Mg lubricants show the largest increase in pressure drop. On the other hand, the Zn lubricant shows very minimal change in pressure drop, despite accumulating nearly twice as much Zn ash. This data is consistent with previous studies showing Zn ash has a minimal effect on pressure drop in the DPF. The majority of the increase in DPF pressure drop is clearly attributed to Ca and Mg.

2.3 POST-MORTEM ANALYSIS PROCEDURE

Following ash loading and DPF performance evaluation, a detailed post-mortem analysis was conducted. First, digital images were taken of the samples and used them to measure the overall ash distribution and thickness. Then the mass of the filter samples was measured in order to calculate the ash packing density and determine its variation with the filter location.

Additional samples were prepared for the SEM analysis. SEM was used in order to investigate ash deposit morphology and the ash distribution using both high resolution imaging and Energy Dispersive X-ray Spectrometry (EDX) for elemental analysis. Based on the prevalent theory, Figure 2.3 shows the expected bulk ash distribution with the additive tracers, forming the hypothesis for this work.

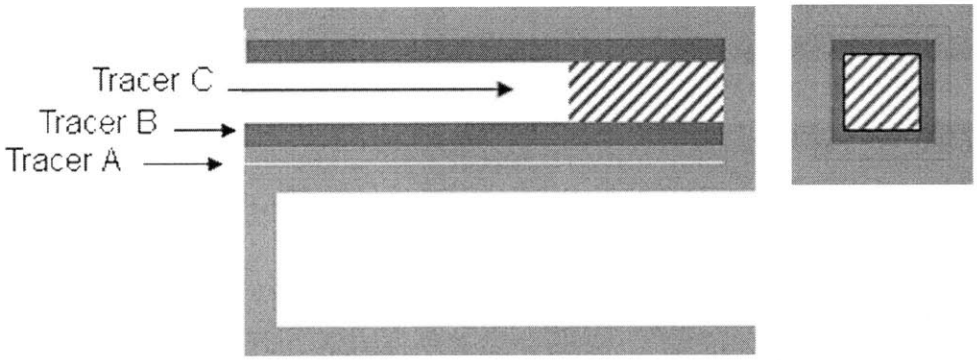

Figure 2.3. Theoretical ash layering along DPF channel.

As shown in Figure 2.3, tracer A, or Ca in this case, is expected to primarily deposit along the channel wall. Then, Tracer B, or Zn may develop a layer on top of the Ca. Finally, it is expected that tracer C, or Mg will primarily form as a plug in the back of the channel, as it was the last lubricant used. Therefore, the plug should theoretically be made of almost completely Mg.

Using all of the analytical methods described above, one can correlate the images and elemental distribution of the ash to the time history of the lubricant tracer. However,

additional measurements may be needed in order to quantify key ash properties (such as shear stress). Finally, the experimental results can be applied to extend the current modeling efforts and better understand the impact of ash on DPF performance.

2.3.1 DPF Sample Preparation

In order to carry out the post-mortem analysis, the DPF was first into small samples. Figure 2.4 shows the location of the different samples.

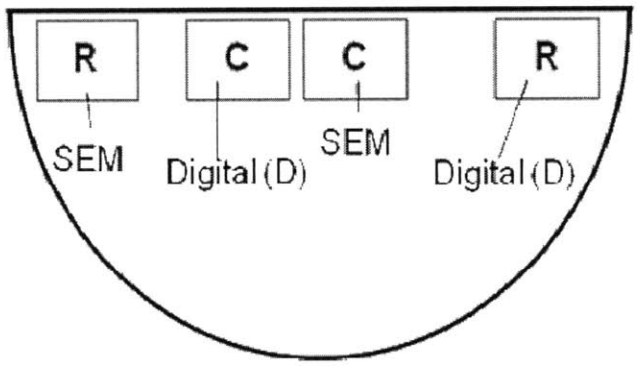

Figure 2.4. Radial location of DPF samples from frontal view in DPF half section.

On either radial edge of the DPF, a row of sample was taken: one for SEM imaging and one for digital imaging (labeled as R or radial samples). Near the center of the DPF, two more rows of samples were removed, one for SEM imaging and one for digital imaging (labeled as C or centerline samples). Figure 2.5 shows the axial placement along the filter of the center and radial SEM samples.

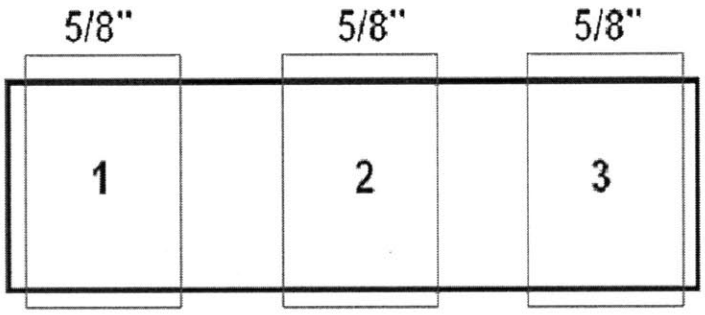

Figure 2.5. SEM samples along DPF length.

For both the radial and center SEM rows, three 0.625" axial samples were removed: one at the front of the DPF, one in the middle, and one at the back, designated as samples 1, 2, and 3, respectively, for a total of six samples per DPF. Each sample contained approximately 88 – 110 cells. Figure 2.6 illustrates the location for the samples used for digital imaging along the length of the filter.

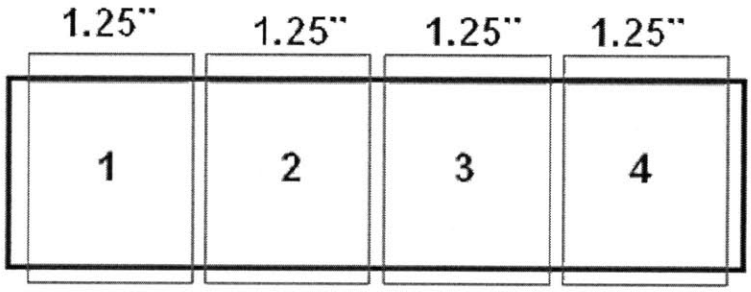

Figure 2.6. Sample locations for digital imaging studies along DPF length.

For the digital image samples, the center and radial rows were each divided into four 1.25" axial samples, making a total of eight samples per DPF. Each sample also consisted of approximately 110 cells.

2.3.2 SEM Sample Designations

For the sake of clarity, the following sample designations, corresponding to the schematic in Figure 2.5, will be used throughout this work:

- C1: centerline, front sample
- C2: centerline, middle sample
- C3: centerline, back sample
- R1: radial/periphery, front sample
- R2: radial/periphery, middle sample
- R3: radial/periphery, back sample

2.3.3 SEM Sample Preparation Procedure

In order to analyze the ash in the SEM, the DPF samples had to be cut to fit the lab crucibles. Then the samples were epoxy mounted in the vertical direction. One important thing to note is that the side to be imaged should be pointing down, as the bottom face will be slightly better for the grind and polish procedure, and the ash will remain more undisturbed than the ash at the top. The ash at the top may be slightly disturbed from the handling of the sample and from the epoxy from the epoxy mounting (which only affects the samples if both sides are to be imaged). Next each mounted sample was ground with 500, 1200, and 4000 grit sand paper, respectively before being polished with a 0.3 μm Al_2O_3 disc (see Appendix for full in depth procedure of epoxy mounting, grinding, and polishing). Finally, each polished sample received a thin carbon layer on the top (side to be imaged). Following sample preparation, they were imaged in a JEOL 5910 SEM and with the EDX elemental analysis (see appendix for full SEM and EDX procedures). This allowed for the imaging of both the actual sample and ash in the channel while simultaneously determining the elemental composition of the ash.

2.3.4 DPF Digital Imaging and Ash Distribution Measurements

For the ash distribution measurements, a high resolution digital image was taken of the front and back of each sample. Then the ash layer thickness was measured at the front and back faces of each individual channel in the DPF samples. Figure 2.7 shows an example of a close up view of the ash deposited in the DPF channels and ash layer thickness measurement methodology.

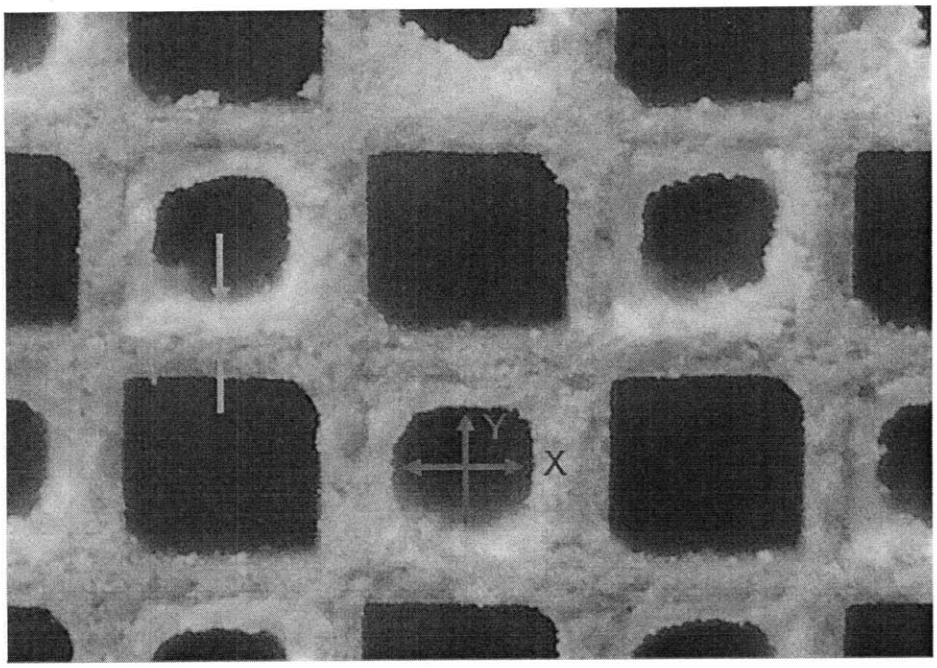

Figure 2.7. Ash thickness measurement methodology

For each sample, channels containing ash in the top two and bottom two rows were measured. There were two measurements for each channel, one in the horizontal direction and one in the vertical direction. The size of the void space was used to determine the ash thickness in each channel, as the channel dimensions were known, and the measurements were averaged to determine the ash thickness for the front and back of each sample. Further, the average thicknesses of interfacing sample faces were averaged in order to reconstruct the ash layer thickness profiles along the length of the filter. Although the shape of the ash deposits in the individual channels changes slightly along the filter length, a square shape is assumed for consistency.

3 EXPERIMENTAL RESULTS

The results of the post-mortem analysis provide information related to the overall ash layer thickness and density, along with the properties of the individual layers. Further detailed line analysis via SEM provided additional information related to the thickness of the individual tracer layers. The following section presents the results of this analysis.

3.1 BULK ASH PROPERTIES

From the digital image samples, data was acquired about the bulk properties and distribution of the ash within the DPF.

3.1.1 Overall Ash Layer Thickness

The overall ash thickness was measured at specific distances along the filter length, described in Section 2.3.3. Figure 3.1 shows the average ash thickness along the DPF.

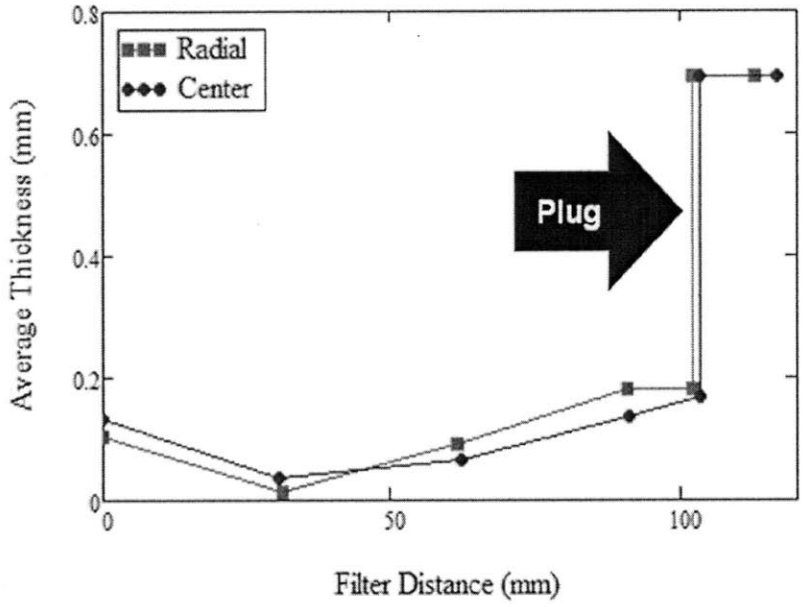

Figure 3.1. Average ash thickness along length of DPF, measured along the DPF centerline and periphery.

The ash layer measurements show that the ash deposited in the DPF begins relatively thick, with layer thicknesses measured at 0.132 and 0.103 mm. The ash then thins out to a minimum in the middle of the DPF. It thickens again until plugging approximately 10 cm from the front face of the DPF. The radial and center samples show similar thickness profiles, although the radial sample begins slightly thinner and then forms a slightly thicker layer before the beginning of the end-plug.

3.1.2 Ash Layer Packing Density

By measuring the mass of each sample with and without ash (by blowing the ash out of the sample with an air hose in between measurements), the mass of the ash was determined. Each sample was weighed three times, and the difference between the ash / no ash averages was recorded as the sample's ash mass. The volume of ash was computed for the ash layer thickness measurements. Finally, the packing density was calculated from the known ash mass and volume. Figure 3.2 shows the average ash packing density along the DPF.

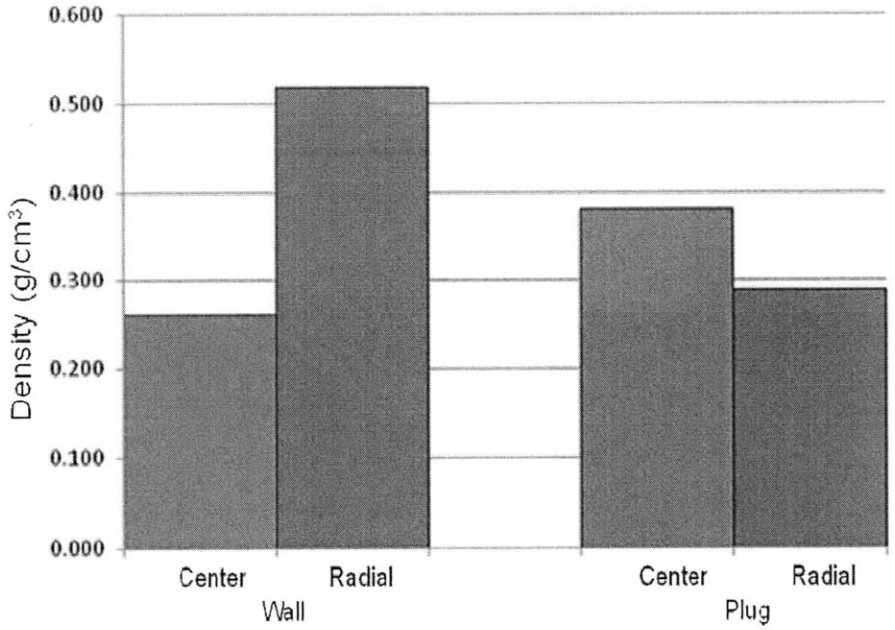

Figure 3.2. Average ash packing density along length of DPF, for center and radial.

There are obvious variations in packing density influenced by the location of ash deposits and the specific layer composition and thickness. For the center samples, the ash in the plug was found to be slightly less dense than the ash along the wall of the DPF channel. However, the ash in the plug of the radial sample is significantly less dense than the ash along the wall of the DPF channel. Much of the observed local packing density variations are attributed to differences in ash layer / plug composition due to variations in the relative proportion of tracer elements in each location.

3.2 ASH LAYER PROPERTIES

Using the SEM and EDX, certain properties of the different ash layers (Ca, Zn, and Mg layers) within the DPF were investigated. This section presents the results of the SEM investigations of the individual layers formed by each of the additive tracers.

3.2.1 Elemental Mapping of Ash Layers in Center Samples

The main tool utilized with the SEM was the EDX elemental analysis, which provides an elemental map of any pre-decided elements in the sample. EDX was used to identify the layering of sulfur, calcium, zinc, phosphorus, and magnesium, which provides information on the evolution of the ash layers with the tracer. This work will look at the layers of the center samples and then the radial samples, going from front to back (front of each sample and then the back of the last sample). Figure 3.3 shows the separate ash layers in the sample from the front of the DPF along the centerline (C1).

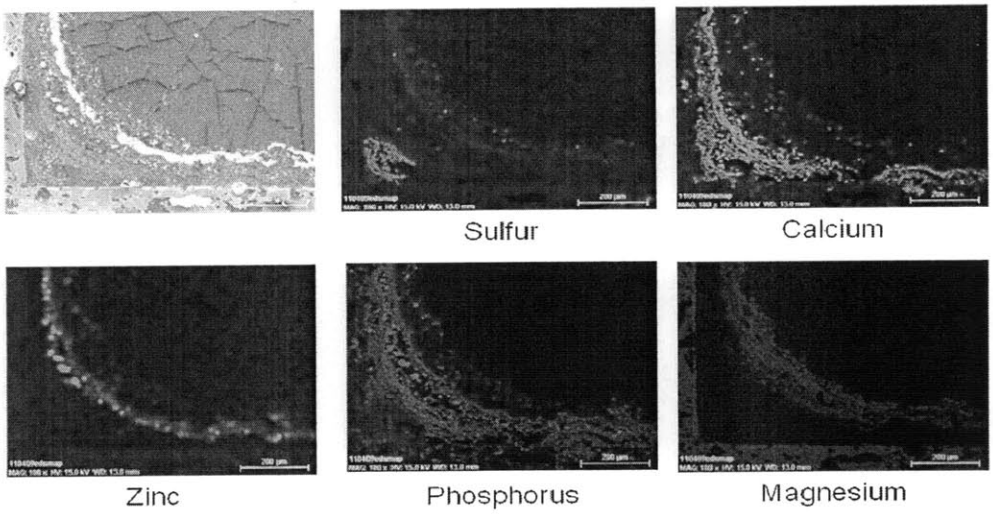

Figure 3.3. C1 EDX images and elemental distribution.

This particular sample shows very distinct layering with the ash from the different lubricants. Even in the SEM image itself, one can see very clear layering. The sulfur is concentrated in the corner of the channel, while the calcium ash shows a nice, thick layer along the wall of the channel. The zinc ash formed in a thin, concentrated layer on top of the calcium layer, yet the phosphorus ash, which comes from the same lubricant as the zinc, created a much thicker and less dense layer, slightly mixed in with the calcium layer. The magnesium ash is found to be on top of the rest of the ash in its own distinct and thick layer. Figure 3.4 shows a superimposed image of the Ca, Zn, and Mg ash layering.

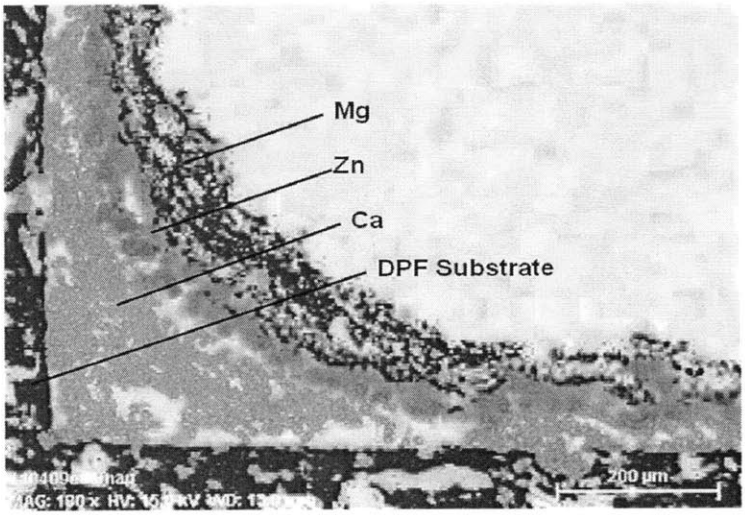

Figure 3.4. C1 superimposed EDX image showing Ca, Zn, and Mg layering.

In this figure, the individual layering of the different lubricants is very clear. The Ca ash appears to have layered quite evenly along the DPF substrate while the Zn ash rests on top in its thin layer and the Mg is on top of that in a thick and less dense layer than the others. Moving along the DPF, Figure 3.5 shows the EDX images for C2.

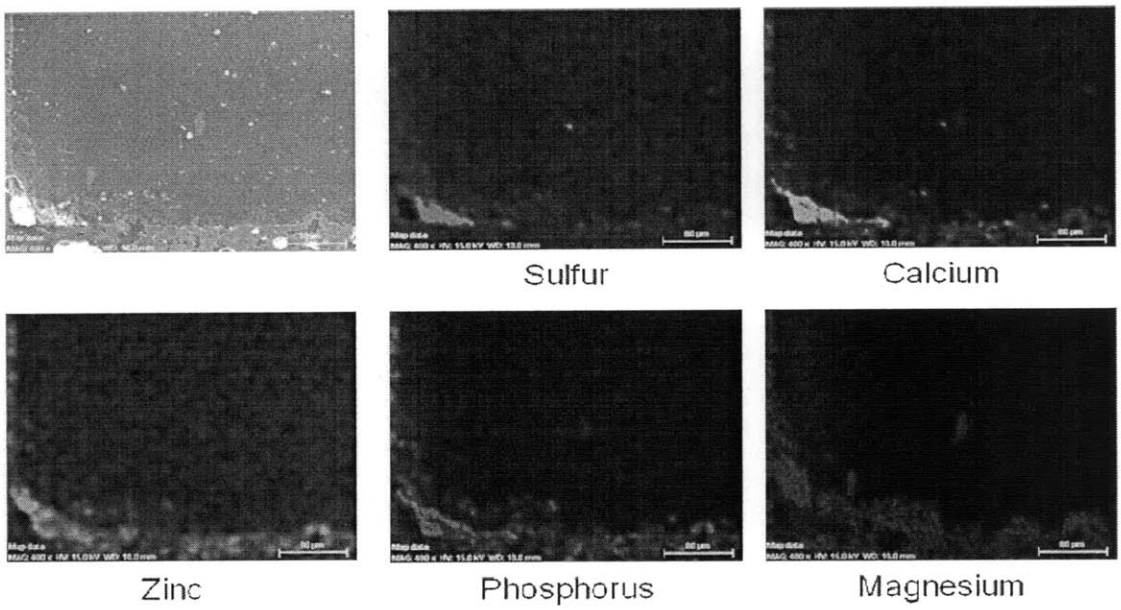

Figure 3.5. C2 EDX images and elemental distribution in the DPF.

Overall, the ash layer in C2 is thinner than that in C1. The sulfur ash is once again concentrated in the corner of the DPF, but this time the Ca ash layer is nearly identical to the S ash layer. In the SEM image, the Ca and S ash also look quite different from the rest of the ash even without use of the EDX. The Zn and P ash layers are nearly identical to each other and are spread along the bottom wall of the DPF. The Mg ash is layered on top of this, mixing slightly with the Zn and S ash in certain areas along the substrate wall. Figure 3.6 shows the superimposed image of the C2 layers, Ca, Zn, and Mg.

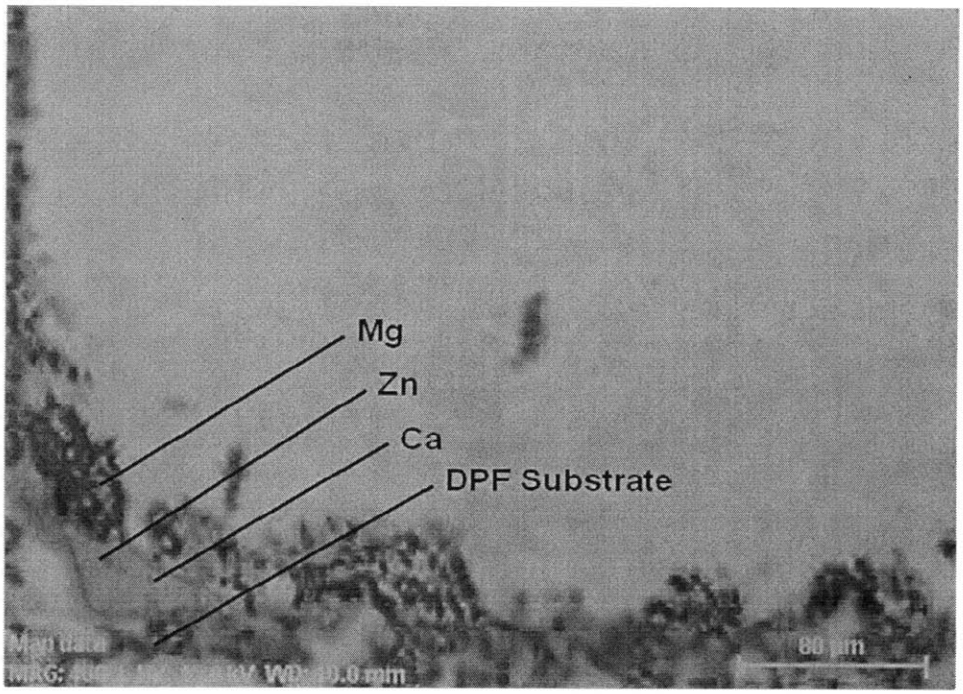

Figure 3.6. C2 superimposed EDX image showing Ca, Zn, and Mg layering.

From the figure, one can actually see that the Ca and Zn ash are concentrated in the corner of the channel. Further the Zn and Ca deposits appear to be sintered together and tightly packed in the corner. The Mg deposits seem to be much more loosely accumulated in a separated layer from the rest of the ash. Figure 3.7 shows the EDX images for the front of C3.

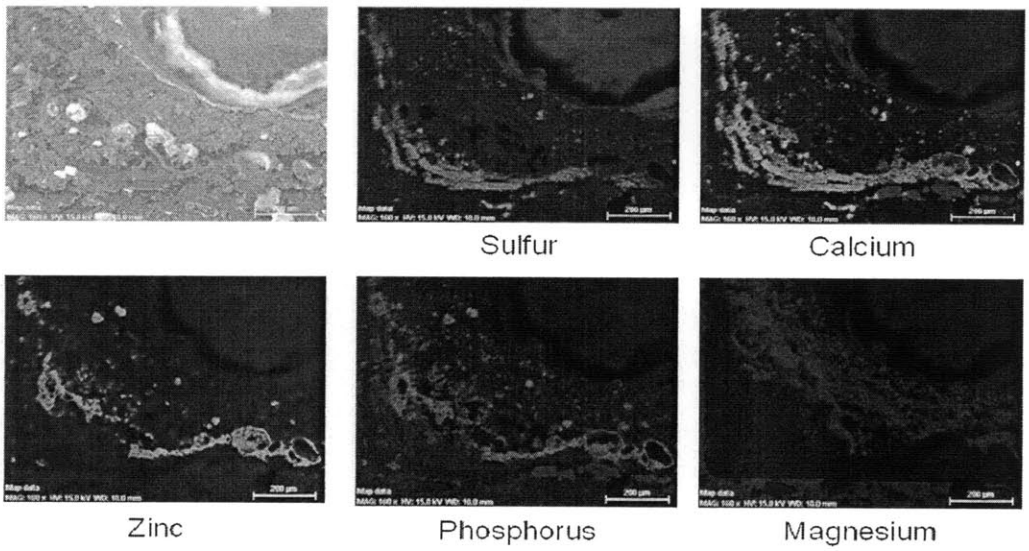

Figure 3.7. Front side of C3 EDX images and elemental distribution in the DPF.

Once again, one can see a thick Ca layer along the DPF substrate with S ash mixed in with most of the Ca ash. The Zn and P ash layers are nearly identical, while the Mg ash creates its own layer on top and actually seems to have formed much of the ash plug. Figure 3.8 shows the superimposed image of the Ca, Zn, and Mg ash.

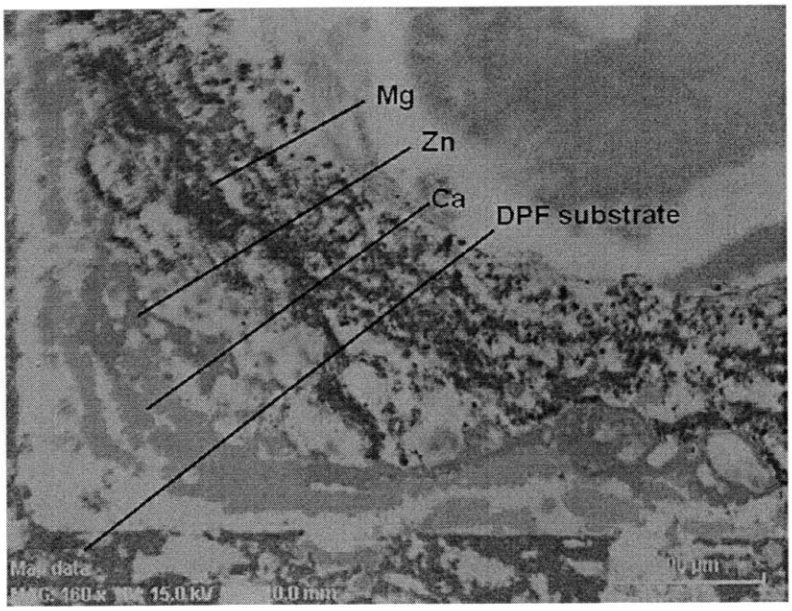

Figure 3.8. Front side of C3 superimposed EDX image showing Ca, Zn, and Mg layering.

The Ca and Zn layers in the front side of C3 appear to have mixed more with each other than in C1 and less so than C2. The Mg ash seems to still have a separate but less dense layer and appears to constitute the actual ash plug toward the front of the plugged area. However, the back of the plug also had to be investigated, as the ash initiating the plug could not be determined purely from the front of the plug. Figure 3.9 shows the EDX images for the back of C3.

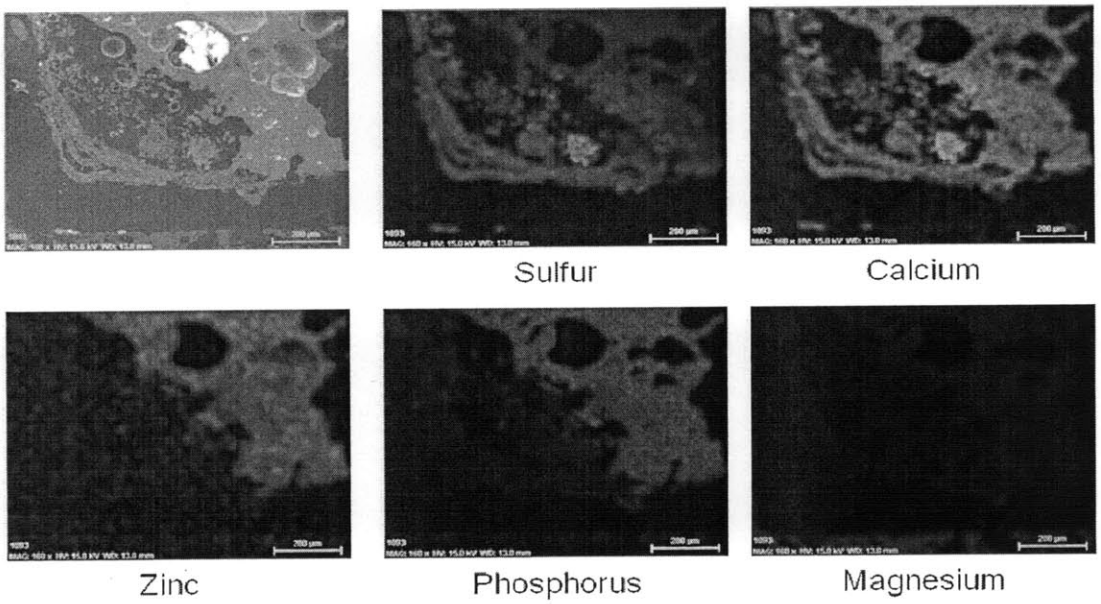

Figure 3.9. Back side of C3 EDX images and elemental distribution in DPF.

According to the figure, the Ca ash appears to constitute most of the back of the plug. Sulfur ash is seen almost only in the Ca ash layer. Zn and P, whose ash layers are identical, are found further away from the DPF substrate and mixed heavily in the Ca ash. From this one can assume that although the back of the plug seem to be made of the ash from the first lubricant, the ash from the second has been pushed back far enough to mix with the first layer. There is also a very minimal amount of Mg ash found mixed in with the rest of the ash, showing that some Mg managed to also get pushed to the back of the plug.

3.2.2 Elemental Mapping of Ash Layers in Radial Samples

The same analysis applied to the DPF samples along the filter centerline was repeated for the radial samples. Figure 3.10 shows the EDX images for Radial 1 (Radial Front Sample).

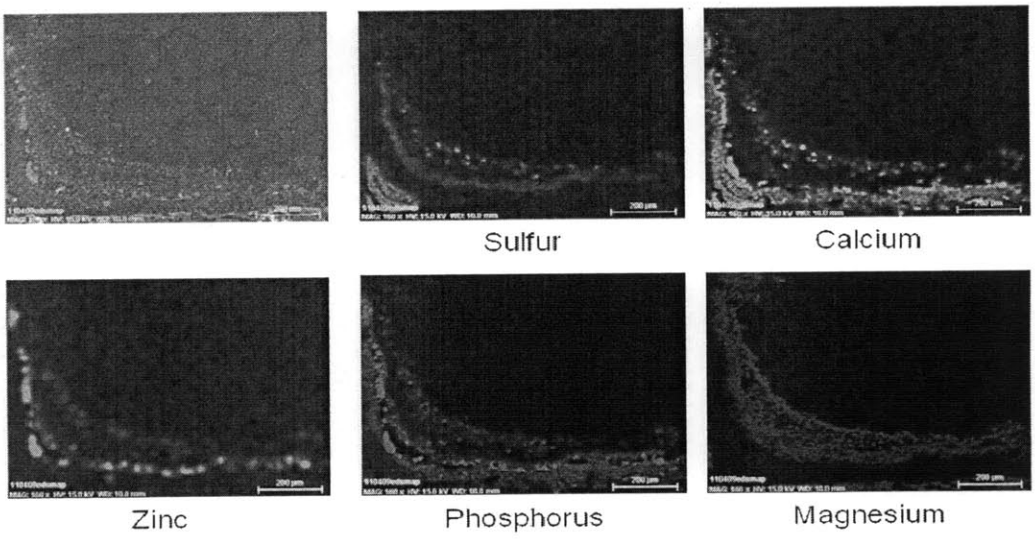

Figure 3.10. R1 EDX images and elemental distribution in the DPF.

The layer formations found in R1 are quite similar to those found in C1. The Ca ash is found along the DPF substrate in an even, thick layer with the sulfur ash mixed in but concentrated in the corner of the DPF. The zinc ash is once again found in a very thin but concentrated layer on top of the Ca layer, similar to C1. Also, the phosphorus ash once again created a thicker layer than the Zn ash, similar to C1. The magnesium ash has also created a thick layer on top of the others. Figure 3.11 shows the superimposed image for the Ca, Zn, and Mg layers.

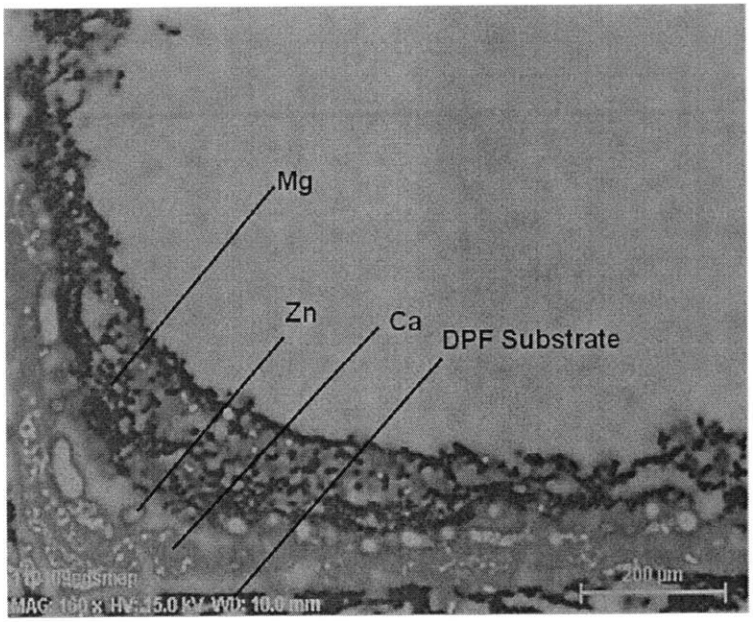

Figure 3.11. R1 superimposed EDX image showing Ca, Zn, and Mg layering.

The superimposed image also parallels that of C1, as the three elements show very clear individual layers evenly distributed along the DPF substrate. Figure 3.12 shows the EDX images for R2.

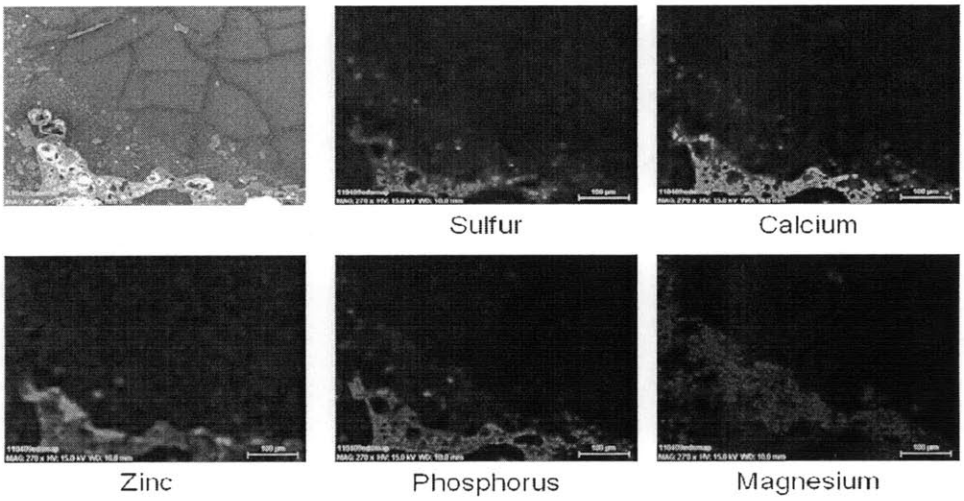

Figure 3.12. R2 EDX images and elemental distribution in the DPF.

As seen in the figure, Radial 2 has very similar layering to Center. The S and Ca layers seem to be identical, as are the Zn and P layers. Further, the S, Ca, Zn, and P appear to have fused or sintered together, and appear to be much denser than the Mg ash. This apparent sintering was observed in the center samples as well, but is surprising given the fact that the DPF temperatures were generally below 700°C during ash loading. Figure 3.13 shows the superimposed image of the Ca, Zn, and Mg layers for Radial 2.

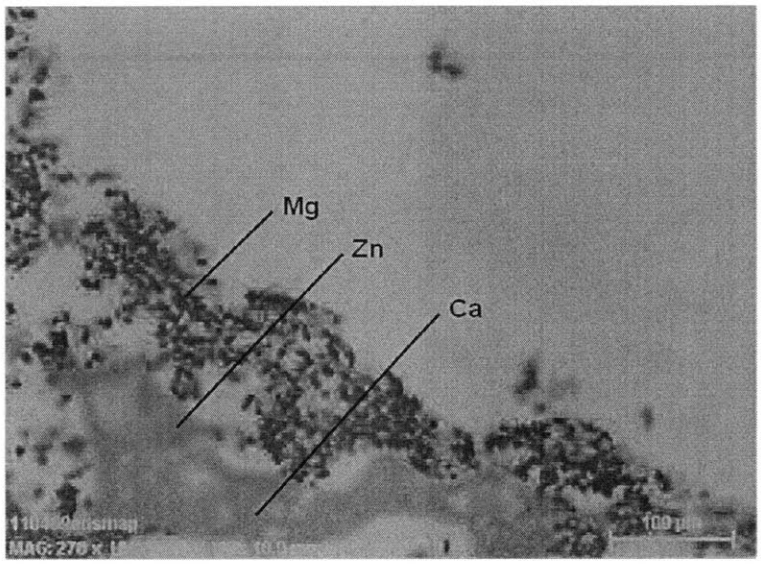

Figure 3.13. R2 superimposed EDX image showing Ca, Zn, and Mg layering.

The figure shows the Ca and Zn deposits to be consistently tightly packed with each other while the Mg deposits remain lightly on top in a separate layer. Additionally, the ash layer appears to be thinner in the middle of the DPF, which supports previous measurements of total ash thickness. Figure 3.14 shows the EDX images of the front of R3.

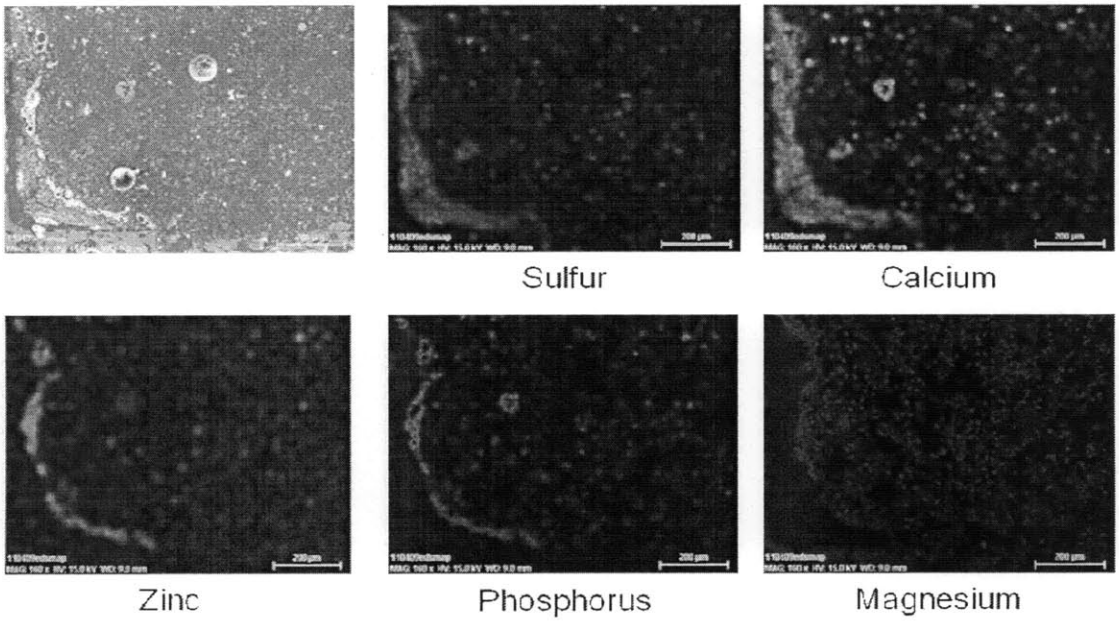

Figure 3.14. Front side of R3 EDX images and elemental distribution in the DPF.

The Ca and S ash, which seem to have nearly identical layers, are evenly layered along the DPF substrate. The Zn and P ash have created a thin layer in the middle together. Further, the plug consists primarily of the final tracer, Mg, which also seems much less dense and concentrated than the other tracer elements. Figure 3.15 shows the superimposed image of the Ca, Zn, and Mg layers.

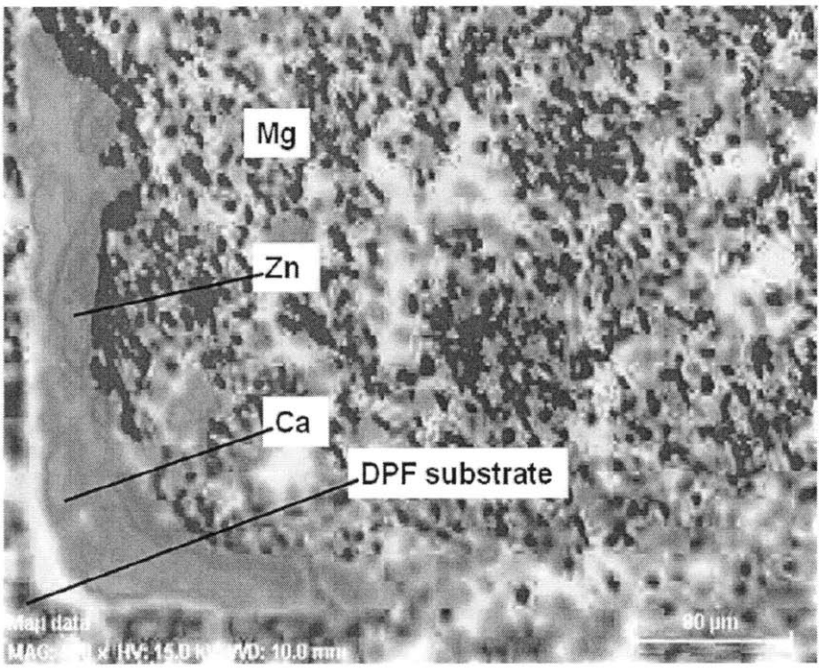

Figure 3.15. Front side of R3 superimposed EDX image showing Ca, Zn, and Mg layering.

As with Center 3, the Ca and Zn ash appears slightly sintered together in a dense layer along the DPF substrate. The plug also consists mostly of Mg ash, which appears to be less densely packed. Figure 3.16 shows the EDX images for the back side of the radial plug.

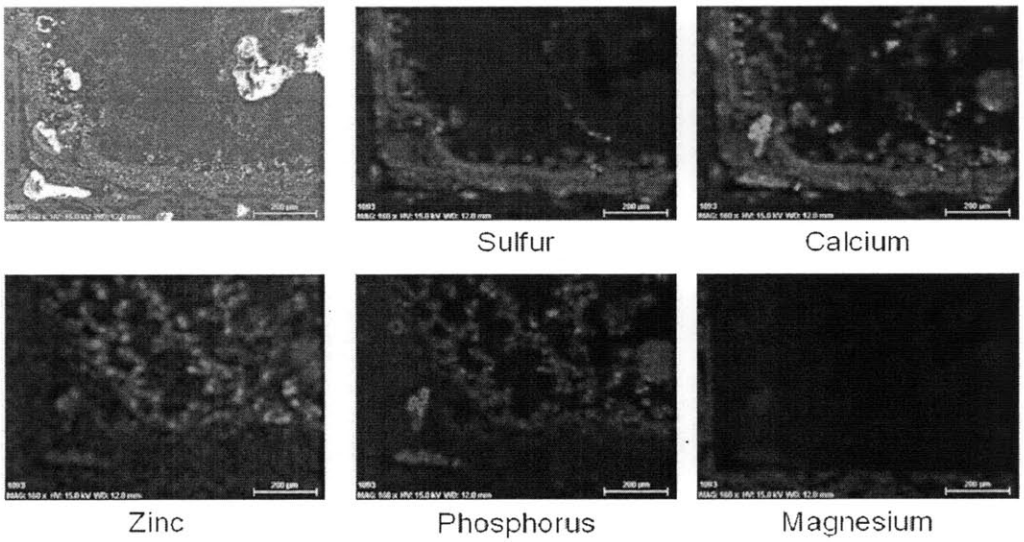

Figure 3.16. Back side of R3 EDX images and elemental distribution in the DPF.

From the figure one can see that the back of the radial plug consists of ash from both the Ca and Zn lubricant. There is also no Mg ash present in the back of the plug. The Ca and S ash, whose profiles are nearly identical, seem to have created a thick layer along the DPF substrate. The Zn and P ash have filled in the rest of the plug. The Zn ash in this sample also appears to be less dense than the Zn ash found in the other samples of this DPF. Once again, there are small traces of Mg ash found in the back of the plug, showing that some (although minimal) of the Mg is pushed to the back of the plug from the front.

The results of the EDX elemental mapping for both center and radial samples show similar trends:

- Each of the ash layers begin as thick, separated layers in the front of the DPF
- The Ca and Zn ash seem to sinter in the middle of the DPF, but show distinctive layering towards the rear of the DPF but before the ash plug
- Despite producing nearly twice as much ash by mass as the other elements, the Zn ash was only found in a thin, concentrated layer (when not sintered with Ca ash) although P ash was much more disperse
- Mg ash deposits are much more loosely accumulated in a separate layer from the other elements.
- Along the channel wall but immediately upstream of the ash plug, all of the tracers can be found in distinct layers. However, the front of the plug itself is made of Mg ash.
- The back of the plug is almost entirely Ca ash, with some apparent Zn ash and a very small trace of Mg ash.

3.2.3 Individual Ash Layer Thickness Measurements

From the SEM EDX images, the thickness of each ash layer was measured. The thickness of each individual layer, identified by the specific tracers, was measured and recorded by. The thickness of the ash deposited in the corners (corner measurements) of the DPF channel and the thickness of the ash deposited along the walls (side

measurements) of the DPF channel were measured. In the following measurements, the individual ash layers (ie, Ca layer, Zn layer and Mg layer) were taken into consideration. Three measurements were averaged in order to determine the recorded thickness. Figure 3.17 shows the layer thickness measurements for the Ca ash.

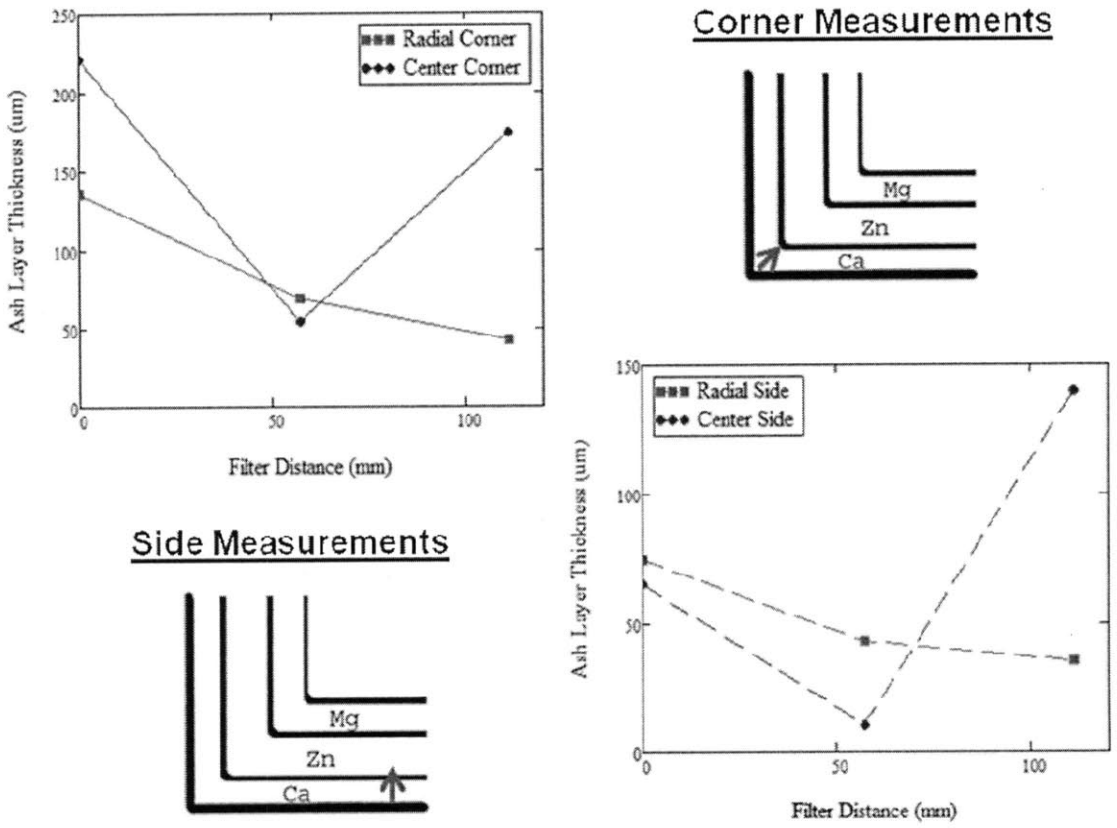

Figure 3.17. Individual ash layer thickness measurements for Ca ash layer.

The corner and side measurements for the Ca show similar trends. The Ca layer begins fairly thick in the front of the DPF. In the center samples, the layer thickness decreases significantly and then increases to approximately the same thickness as in the front of the DPF (in the corner) or thicker than in the front of the DPF (for the side of the channel). In the radial samples, there is a constant decrease in thickness throughout the length of the DPF. Figure 3.18 shows the layer thicknesses for the Zn ash.

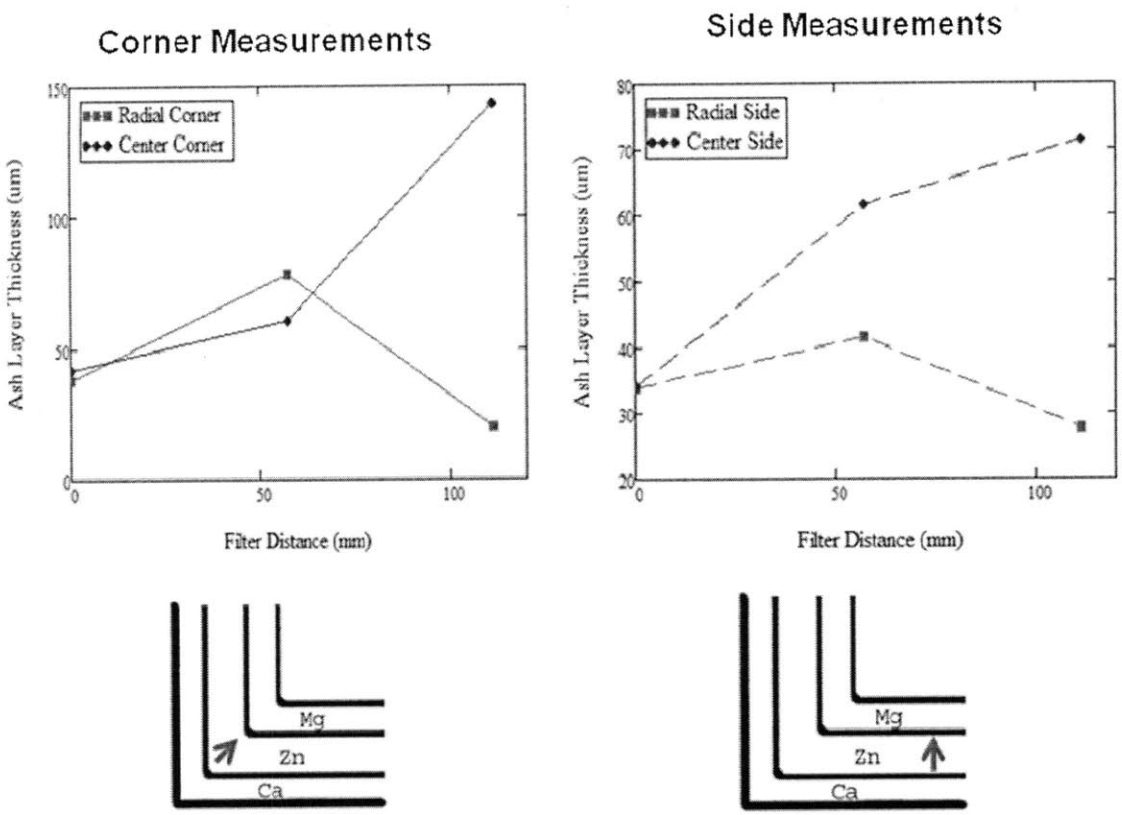

Figure 3.18. Individual ash layer thickness measurements for Zn ash layer.

As shown in the figure, the Zn ash shows the same general trends for the corner and side measurements. In the center samples, the Zn layer thickness constantly increases along the length of the DPF. In the radial samples, the Zn layer actually becomes thicker in the middle of the DPF and then thins out again toward the back of the DPF. Besides the layer in C3, the Zn layer is relatively thinner than the other layers. Figure 3.19 shows the layer thickness for the Mg ash throughout the DPF.

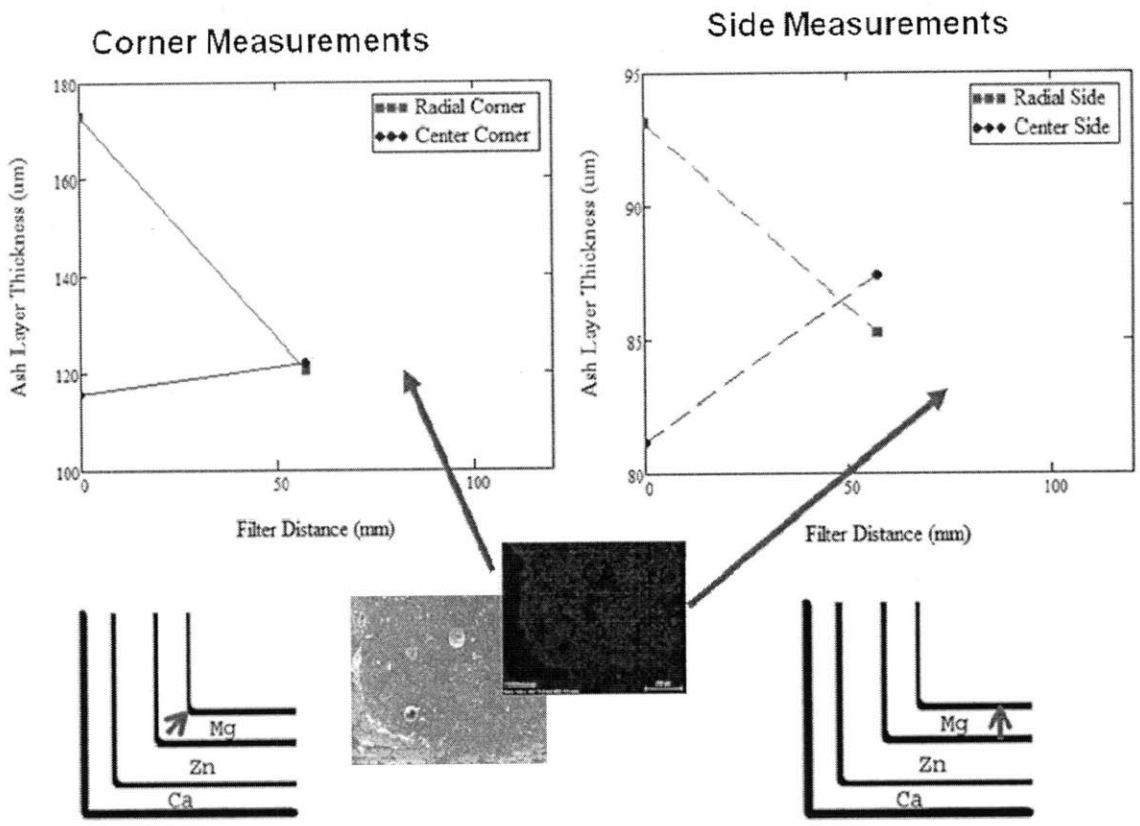

Figure 3.19. Individual ash layer thickness measurements for Mg ash layer.

Once again, the corner and side measurements prove to be similar to each other. In the center samples, the Mg layer thickness increases slightly throughout the DPF while a noticeable decrease in the thickness of the Mg layer is observed in the radial samples. In both C3 and R3, approximately 10 cm from the filter inlet, a plug formed. Therefore no third measurement is present.

The results of the individual ash layer thickness measurements show:

- Each individual layer thickness increased between the front and back of the DPF along the centerline
- Each individual layer thickness decreased from the front to the back of the DPF in the radial samples
- The Ca layer is thinner in the middle along the centerline than the front or back

- The radial and center layers are closer in thickness in the front and middle of the DPF than in the back of the DPF

3.2.4 Cumulative Ash Layer Thickness Measurements

The following section presents the cumulative ash layer thickness measurements referenced to the DPF substrate for ash accumulated in the corner of the channel as well as along the channel walls. Figures 3.20-3.21 show ash layer evolution for the corner and side (respectively) of the radial samples.

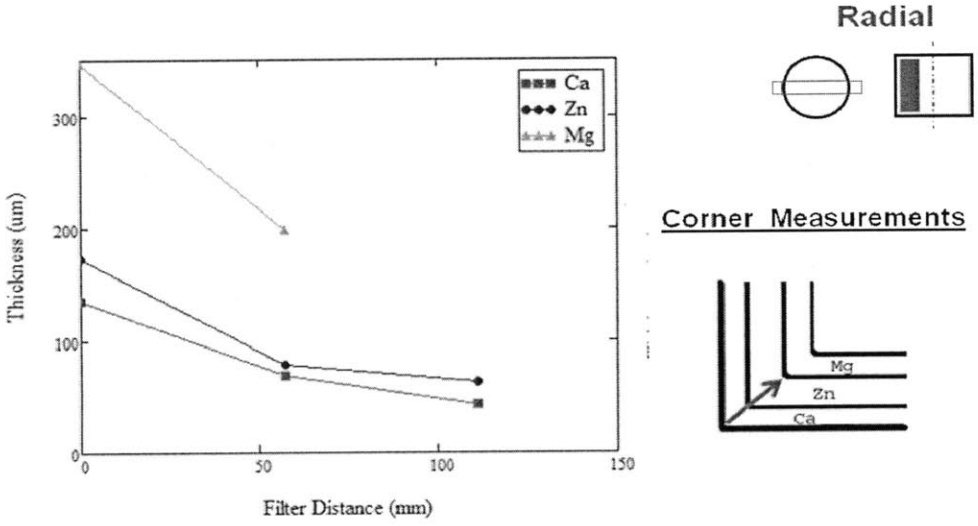

Figure 3.20. Cumulative ash layer thickness along DPF for radial corner.

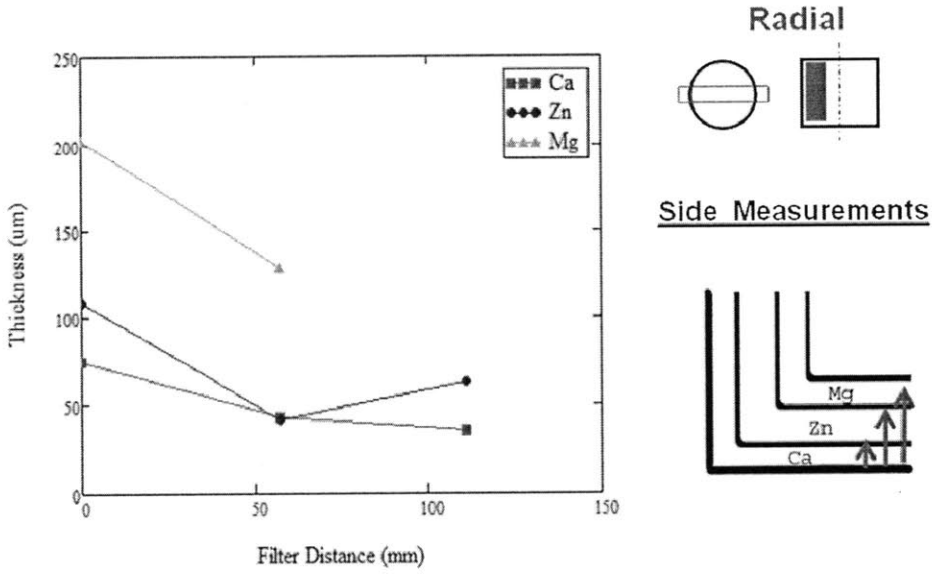

Figure 3.21. Cumulative ash layer thickness along DPF for radial side.

In the corner of the radial samples, the overall ash is observed to decrease along the length of the DPF. Relative to the side of the DPF substrate, the overall ash thickness decreases in the middle of the filter with a slight increase leading into the plug. Once again, despite having the most ash by mass, the Zn shows the thinnest ash layer in the radial samples. The Mg also appears to have the thickest layer and to be the least densely packed. Figures 3.22-3.23 show the corner and side measurements, respectively, of the different ash layers for the center samples.

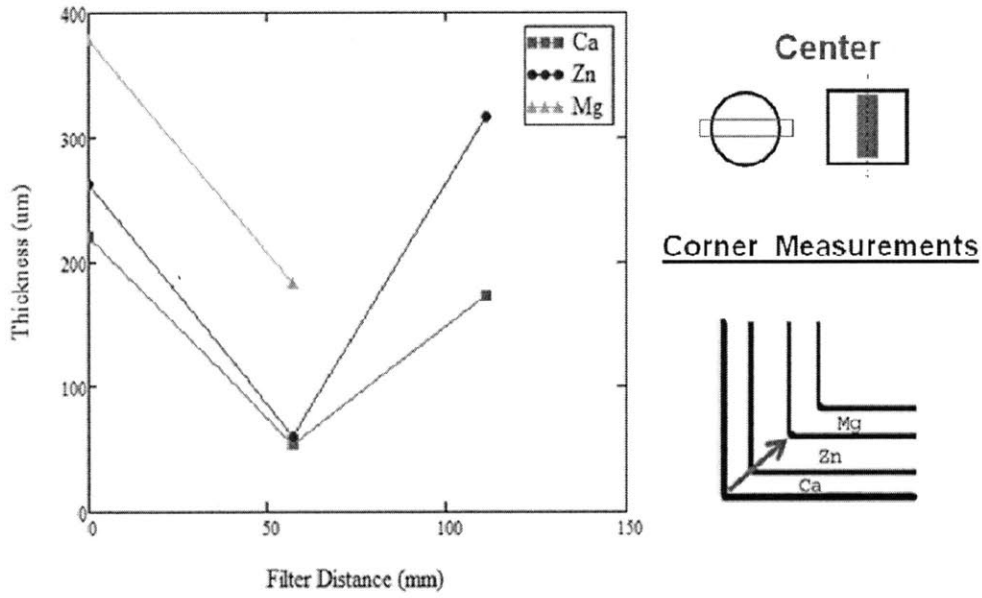

Figure 3.22. Cumulative ash layer thickness along DPF for center corner.

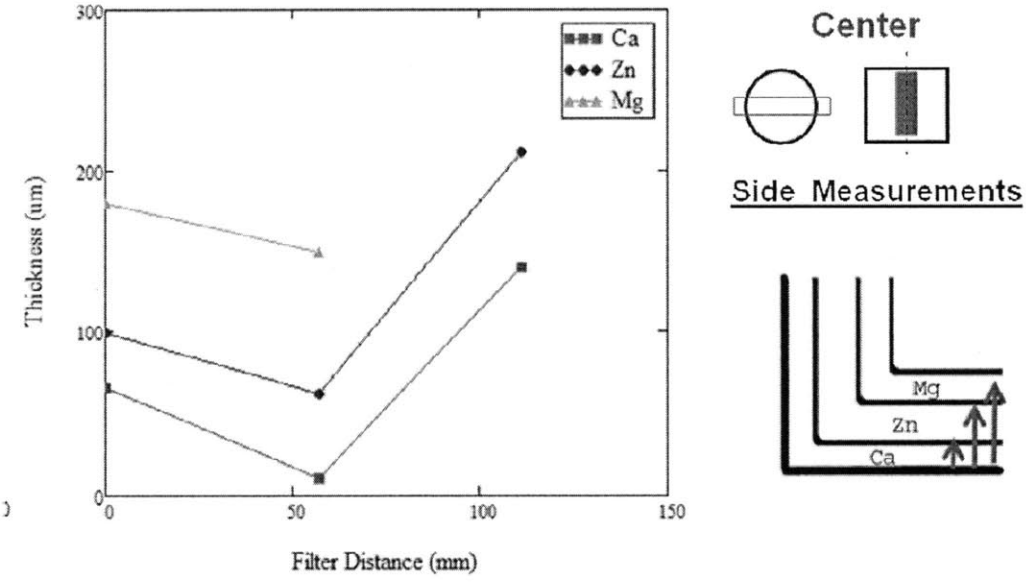

Figure 3.23. Cumulative ash layer thickness along DPF for center side.

In the center samples, the overall ash layer thickness decreases in the middle of the DPF and then increases again leading into the ash plug in the back of the DPF. In the same fashion, the individual layers are thinnest in the middle of the DPF. The Zn layer also remains thinner relative to the Ca and Mg layers, while the Mg layer is thicker relative to the Ca and Zn layers. Additionally, the Zn layer appears to be thicker along the centerline of the DPF. Overall, the ash layer and distribution profiles show similar trends for all of the samples.

The results for the cumulative ash layer thickness show:

- All of the ash layer thicknesses decrease in the middle of this particular DPF
- The radial layer thicknesses continue to decrease in the back of the DPF while the center layer thicknesses actually increase
- The Mg layer is the thickest of the three ash layers
- The Zn layer is the thinnest of the three ash layers

3.2.5 Line Analyses

The distribution of the trace elements in the ash layer was also quantified using the EDX line analysis with the SEM. The line analysis tool uses similar technology to the mapping/imaging in order to quantify the concentration and thickness of different elements along a chosen path (represented by an arrow drawn on the SEM image). A line analysis was conducted from both the corner and side of the substrate toward the center for each sample. Figure 3.24 shows the line analysis from the corner of C1.

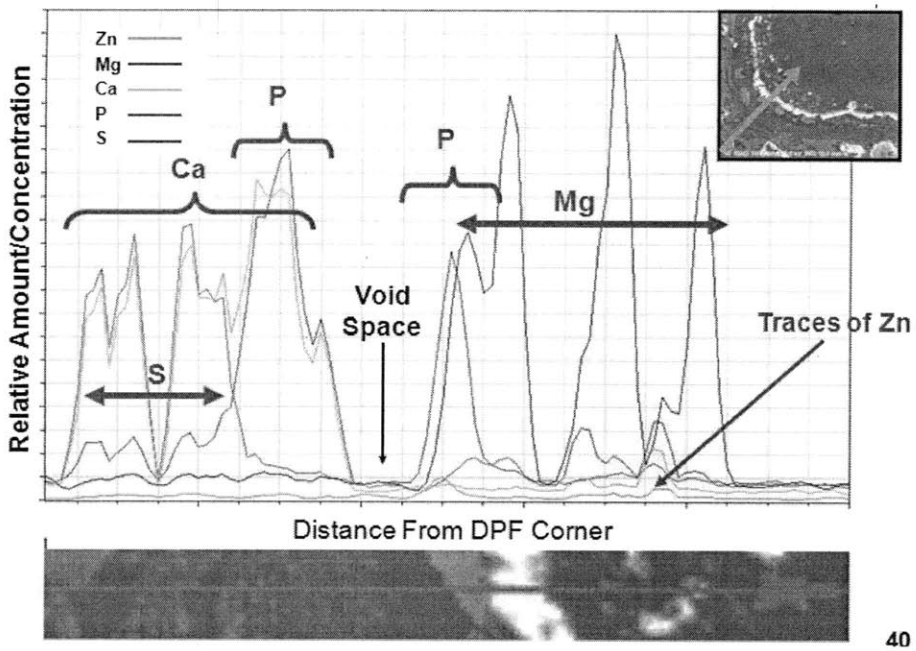

Figure 3.24. Line analysis and ash layer profile for C1 corner.

In the corner of Center 1, the Ca has formed a relatively thick layer, containing both S and P. A small void space is observed before P appears in a thin layer. Mg is then present for the rest of the ash layer in varying concentrations. Although there are traces of Zn in the ash, there is no large concentration that can be identified as a distinct layer of Zn ash. Figure 3.25 shows the side line analysis of C1.

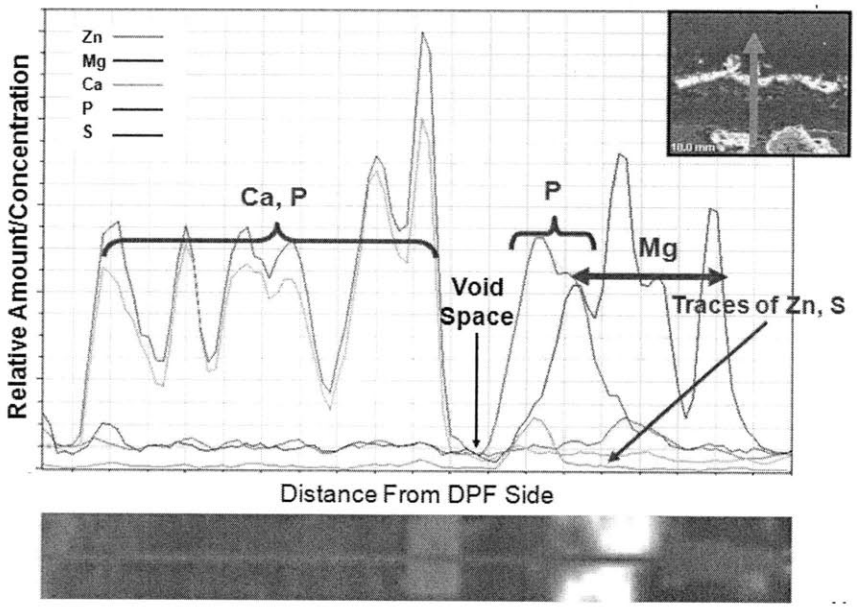

Figure 3.25. Line analysis and ash layer profile for C1 side.

According to the figure, there is a large Ca and P layer, with nearly identical concentration profiles. Above that is a small void space followed by a thin P layer. At the edge of the P layer, a Mg layer appears and constitutes a large, although smaller than the Ca and P, layer on top of the rest. A relatively large amount of Zn is found at the bottom edge of the Mg layer, but the amount of Zn and S present could still only be considered as traces of the elements rather than layers. Figure 3.26 shows the line analysis of the corner of C2.

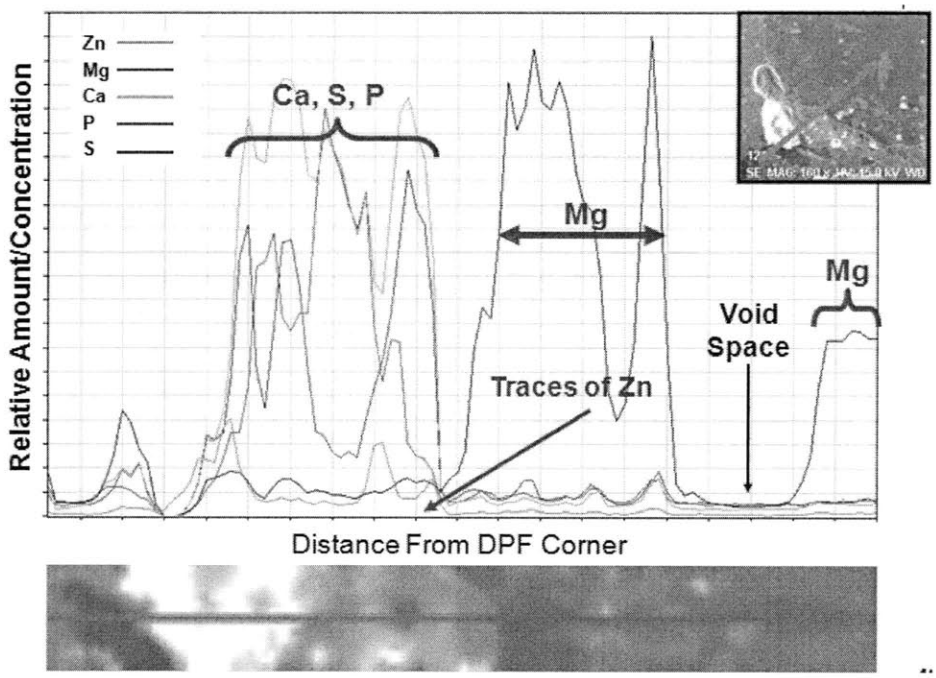

Figure 3.26. Line analysis and ash layer profile for C2 corner.

From the corner of Center 2, there is a thick layer of Ca, S, and P mixed together. There are also some traces of Zn present within this layer. On top of that is a fairly even layer composed primarily of Mg ash, which also contains a void space. Figure 3.27 displays the line analysis for C2 from the side of the DPF substrate.

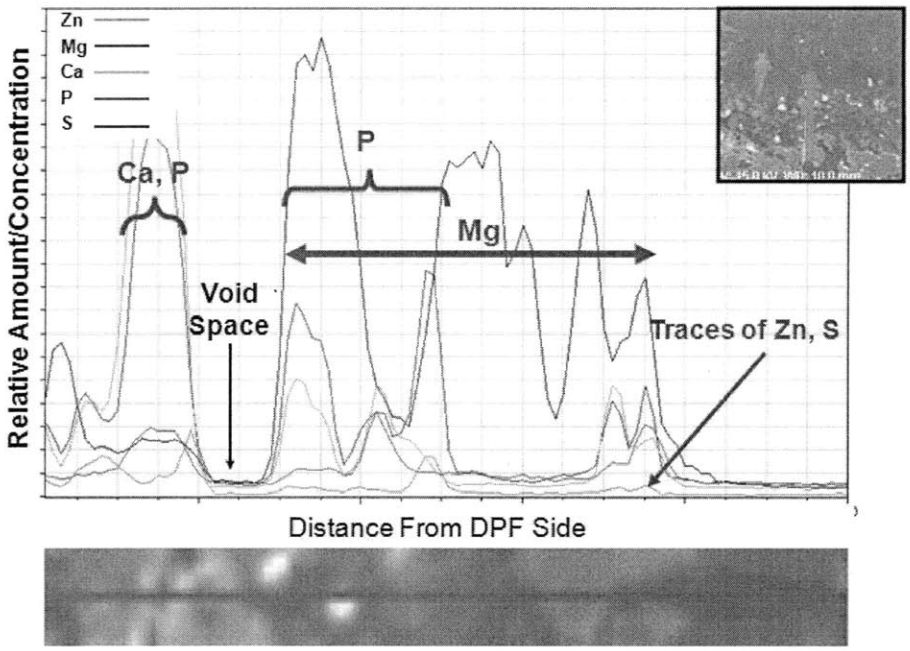

Figure 3.27. Line analysis and ash layer profile for C2 side.

Immediately next to the DPF substrate is a layer of Ca and P ash, mixed evenly together. This Ca and P layer is followed by a small void space before a very thick layer consisting mostly of Mg ash. There is also some P and Ca found at the bottom of this layer, with traces of Zn and S found throughout the whole ash layer. Figure 3.28 shows the line analysis for the corner of C3.

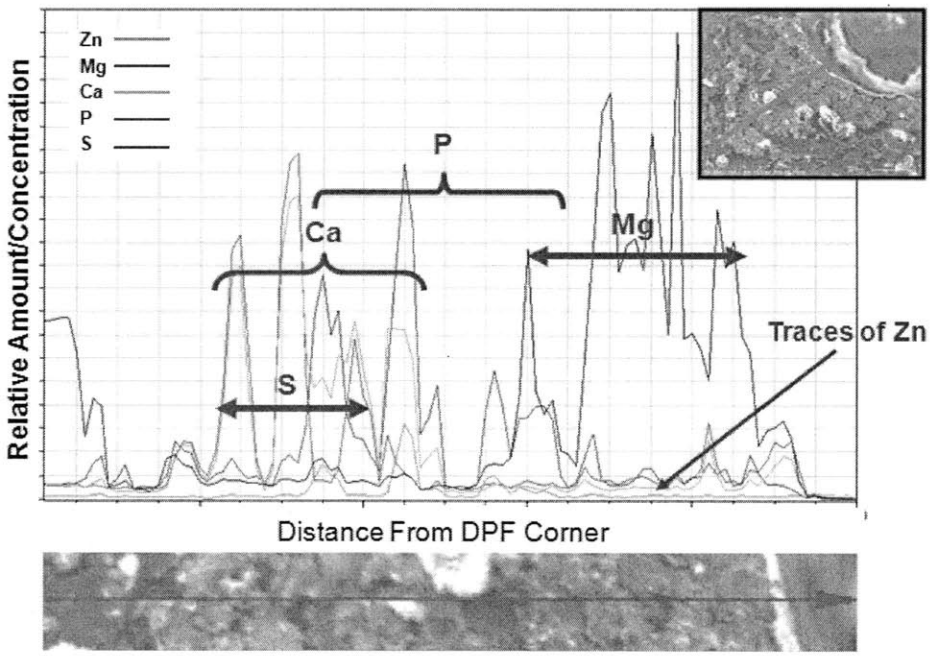

Figure 3.28. Line analysis and ash layer profile for C3 corner.

Moving radially inward from the corner of C3, there is a relatively thick layer of Ca present with S ash mixed in the base of the layer. The P layer appears toward the edge of the S layer. The Mg layer is also found toward the center of the channel in the plug. Although there are traces of Zn throughout the analysis, there is no definite layer of it. Additionally, the plug seems to be made of almost purely Mg with very little trace of any other elements. Figure 3.29 shows the line analysis for C3 from the side of the DPF substrate.

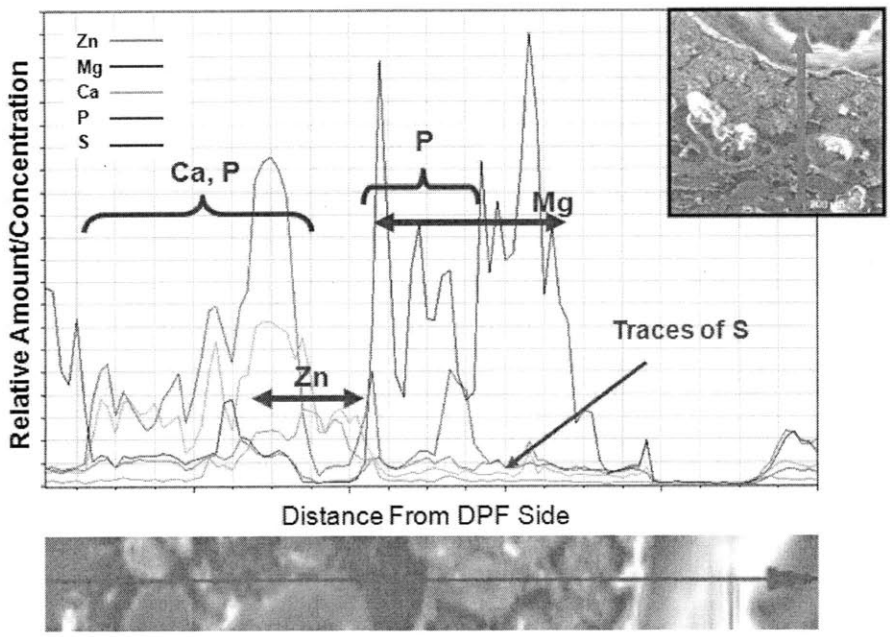

Figure 3.29. Line analysis and ash layer profile for C3 side.

In C3, there is a thick but not very concentrated Ca and P layer. Toward the top of the layer, there is actually a small layer of Zn, also not very concentrated. Above all of this is very thick layer of Mg (the ash plug) with some small amounts of P ash mixed in and traces of S ash present too.

In a similar fashion, the line analyses were carried out for all of the radial samples. Figure 3.30 shows the line analysis for the corner of R1.

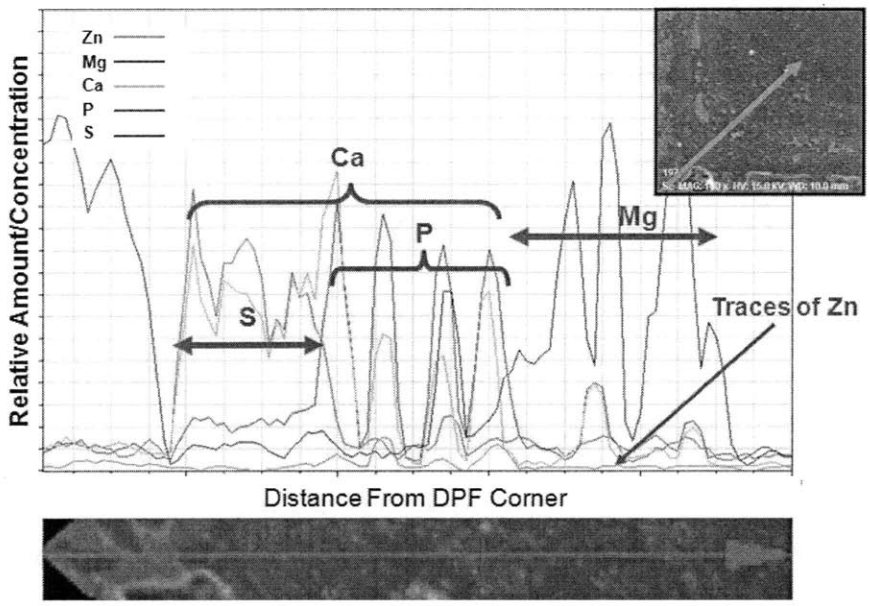

Figure 3.30. Line analysis and ash layer profile for R1 corner.

In R1, there is a very thick Ca layer. Within the layer are a S layer near the substrate and a P layer next to it. There is also a thick Mg layer of varying concentration next to the rest of the ash. There are traces of Zn ash present throughout the DPF, but there is not a high enough concentration to constitute an actual layer. Figure 3.31 shows the line analysis from the side of R1.

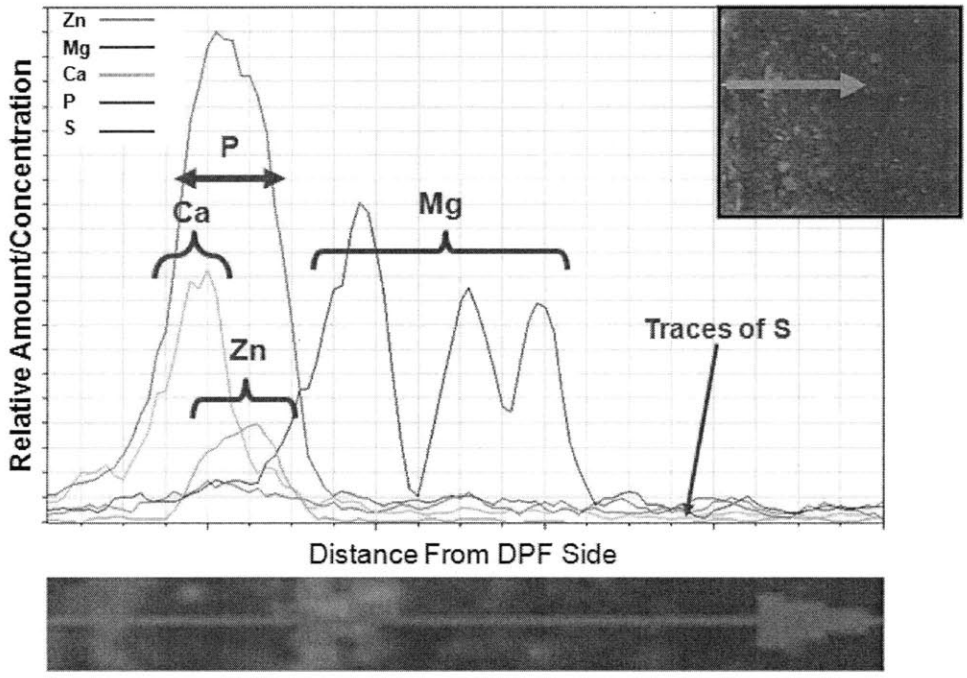

Figure 3.31. Line analysis and ash layer profile for R1 side.

From the side of R1, there is definite layering of first the Ca ash, Zn ash, and then the Mg ash. Although they appear in layers, they seem to mix a small amount at the interface between the layers. A large concentration of P ash is found within the same layers of the Ca and Zn ash. There are also traces of S ash but no actual layer of S present. Figure 3.32 shows the line analysis from the corner of R2.

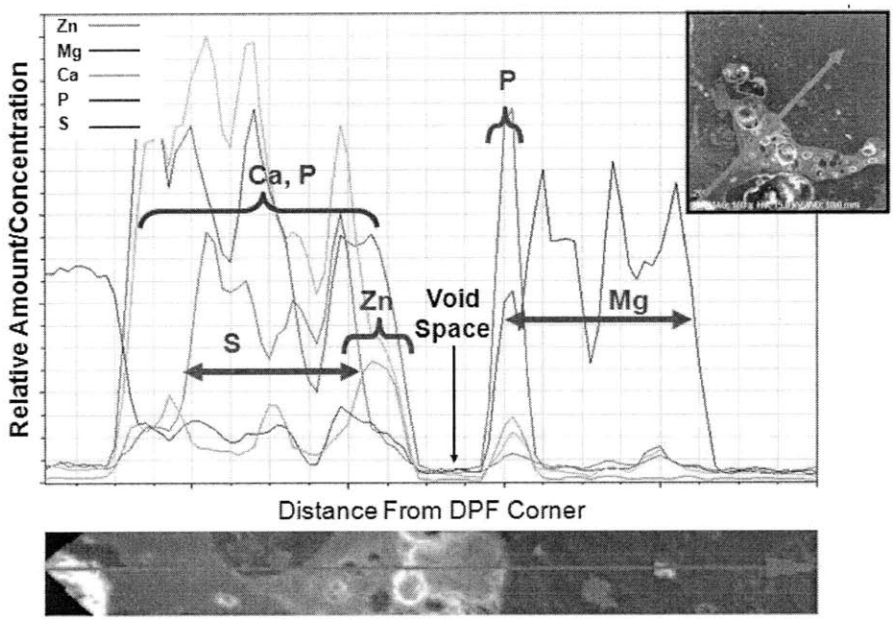

Figure 3.32. Line analysis and ash layer profile for R2 corner.

In the corner of R2, there is a thick and highly concentrated Ca and P layer with S ash mixed in and a small – although larger than any previous sample – concentration of Zn ash mixed in too. Then there is a small void space with a thin but highly concentrated P layer and a thick Mg layer. Figure 3.33 shows the line analysis from the side of R2.

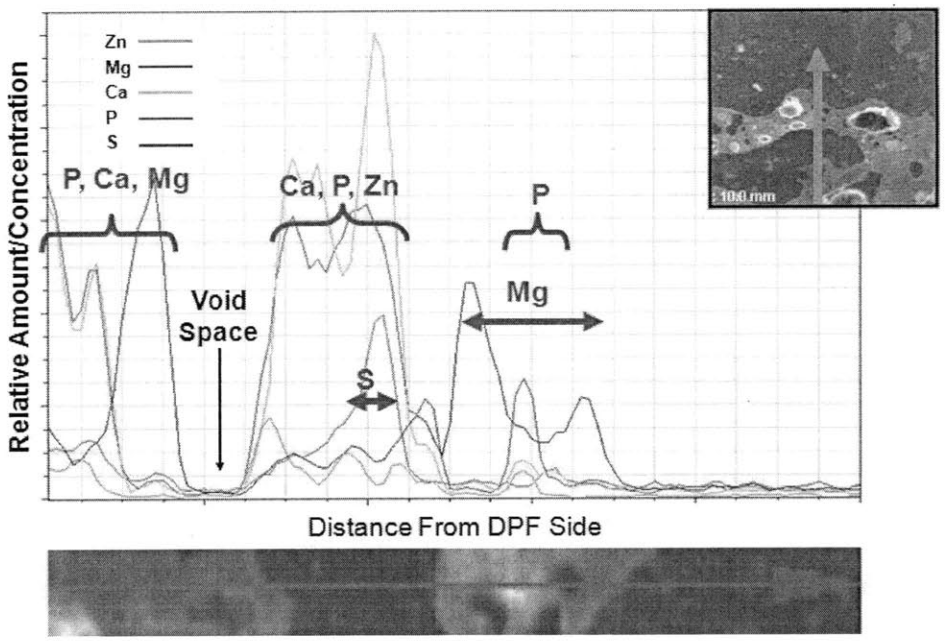

Figure 3.33. Line analysis and ash layer profile for R2 side

On the side of Radial 2, there is a layer of P, Ca, and Mg ash. Above that layer are a void space and then a layer of Ca, P, Zn, and S ash. The Ca and P ash also have similar concentrations. Above that is a layer of Mg with a small amount of P ash in the middle of it. Figure 3.34 shows the corner line analysis for the final sample, Radial 3.

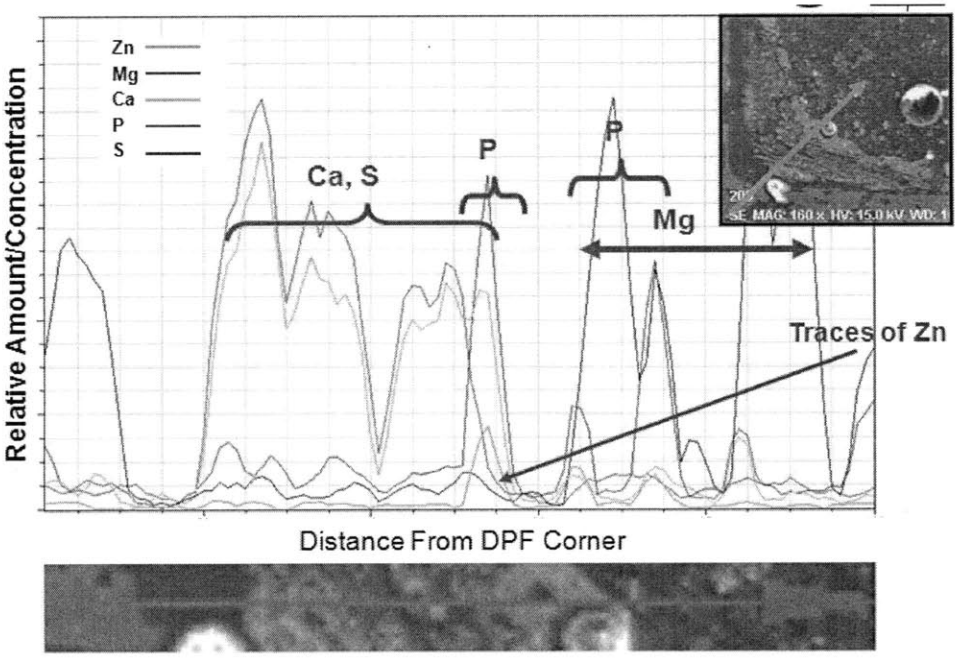

Figure 3.34. Line analysis and ash layer profile for R3 corner

In the corner of R3, there is a thick Ca and S layer, with concentration almost identical to each other. Then there is a small P layer that has traces of Zn in it. After a very small void space, there is a thick layer of Mg showing the edge of the ash plug. Figure 3.35 shows the side line analysis for R3.

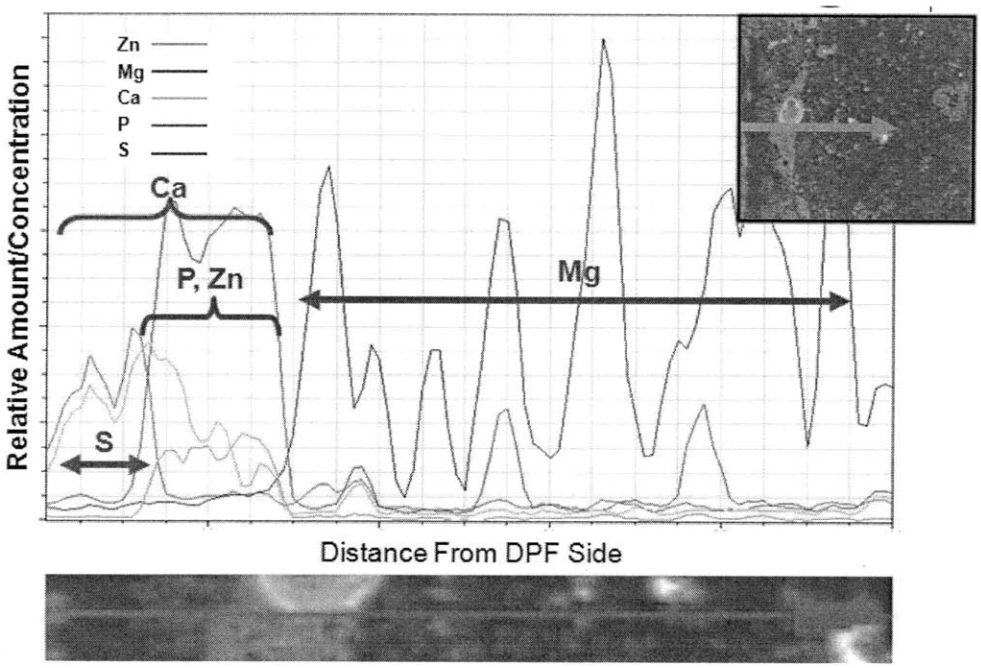

Figure 3.35. Line analysis and ash layer profile for R3 side.

In Radial 3, a thinner Ca layer is found on the DPF substrate. A similar S layer is found in about the first half of the Ca layer. Next to the S layer, but still inside of the Ca layer, P and Zn layers of equal thicknesses but varying concentrations are present. Next to this layer of mixed ash is a separate layer of Mg indicating the edge of the ash plug.

Although the line analysis presents a high level of detail, a number of distinct trends were observed and are described as follows:

- Ash layer evolution is consistent with the time history of tracer application (Ca, Zn, Mg).
- There are two main ash layers present. A base layer made of Ca ash mixed with S and/or P ash and a top layer made of Mg ash
- The S ash seems to be mostly found either closest to the substrate within the Ca layer or nearly identical to the entire Ca layer

- The P ash seems to typically collect at the edge of the Ca layer, away from the substrate, and is sometimes seen to penetrate into the edge of the Mg layer.
- Zn ash, although usually found in low concentrations, is typically observed between the Ca layer and the Mg layer, and is rarely observed as a separate layer.
- The Mg layer typically forms its own layer, sometimes with small traces of P, S, or Zn.
- Void spaces of some sort typically appear between the Ca and Mg layers, supporting low packing density measurements and indicating highly porous morphology

4 Conclusions

Overall, the experiments conducted in this work used three different additive tracers in order to ash load the DPF. From the post-mortem analysis, the overall ash layer thickness and the packing density were measured along the length of the DPF. SEM EDX was also applied to map the different layers of ash (Ca, Zn, Mg). The elemental maps were further used to measure the individual and cumulative ash layer thicknesses. Finally, SEM line analysis was used with each of the samples in order to analyze the relative concentration and thickness of each element in the ash layers.

Data from the different/independent measurement methods is consistent. The location and nature of the individual ash layers observed in the EDX images is supported by the data from the line analysis. Also, the average total ash layer thickness (200 μm) matches the approximate sums of the individual ash layer measurements (between 50 and 100 μm). Therefore, the data was found to be consistent based on the different and independent tests conducted.

Several major conclusions can be drawn from the post-mortem analysis in conjunction with the correlations with the models and DPF performance data:

- Lubricant additives have been successfully applied as an effective method to track the evolution of ash deposits in the DPF.
- Unlike the Ca and Mg ash, the Zn ash did not increase pressure drop in the DPF. The Mg ash appeared to be the least densely packed. On the other hand, Zn ash was more concentrated into thin layers, yet the P ash was much more dispersed. These factors may make Zn ash ideal for packing in the ash plug at the back of the DPF, but additional detailed investigation is needed.
- The front of the ash plug consisted mostly of Mg ash (the third tracer) while the back consisted mostly of Ca ash (the first tracer), indicating that the plug began to form during application of the first tracer and continued to build over the course of the ash loading process. However, there were some noticeable amounts of Zn ash and very minimal amounts of Mg ash in the back of the plug. This indicates

that the Ca portion of the plug was thin enough for Zn ash to easily penetrate to the back of the plug, and that the Zn ash layer also seemed thin enough for the Mg to slightly penetrate to the back of the plug. If true, this would show that even though the plug began to form with the onset of ash deposition in the DPF channel, the plug formed very slowly until the walls reached their critical thickness. Therefore, this critical thickness on the walls would play a major role in the formation of most of the ash plug.

- Even though Ca and Zn ash appeared as their own, separate layers in the front of the DPF, there was possible sintering between the two types of ash in the middle and somewhat in the back of the DPF. These potentially sintered areas were also very easily distinguishable from the rest of the ash in the normal SEM images. This may imply some Ca and Zn agglomerates present in the ash, which were responsible for the apparent decrease in ash layer thickness in the middle of the DPF.
- Void spaces were found between several of the different layers in the SEM line scans. Although the void spaces varied greatly in size, they were present in nearly all of the samples. These support the low packing density measurements and indicate that the ash formed highly porous layers. A reduction of void spaces in the ash-plug could possibly increase the packing density of the plug and reduce the effective plug length, providing a significant pressure drop benefit. This will be the focus of subsequent studies.

The conclusions drawn in this work are important for several reasons. Overall, they are all important in understanding the formation of ash layers and plugs, and understanding them is the first step toward being able to control ash properties and optimize DPF performance. The method of using different tracer lubricants can be extended and reordered to further investigate different key ash parameters and characteristics. Knowing certain characteristics of the different types of ash (from the different tracers), such as concentration, typical thickness, and packing density, can allow for certain elements to be utilized to create thinner layers and smaller plugs. Sintering of elements may also affect the ash properties, determining what elements can actually be used

together. Finally, the elemental make up of the plug is extremely important in understanding how the plug is formed, which can be utilized to control the size and density of the plug.

4.1 FUTURE WORK

While the present work made significant progress in understanding ash distribution and layer characteristics in the DPF, several areas require additional investigation:

- In order to better quantify the ash critical shear stress and mobility, additional test methods are needed.
- Further investigation could be carried out by repeating the experiment with the lubricant tracers run in a different order to investigate the effects, if any, the order of additive tracer application has on the final results (ie. if the thin nature and high concentration of the Zn ash layer was due to characteristics of Zn itself or of being the second tracer).
- The plug needs to be investigated further in order to determine the specific composition of the tracers along the length of the plug. This study shows the front of the plug to be Mg and the back to be Ca, but further study could determine how much of the plug is formed by each lubricant. Figure 4.1 shows two possible hypotheses for the plug formation.

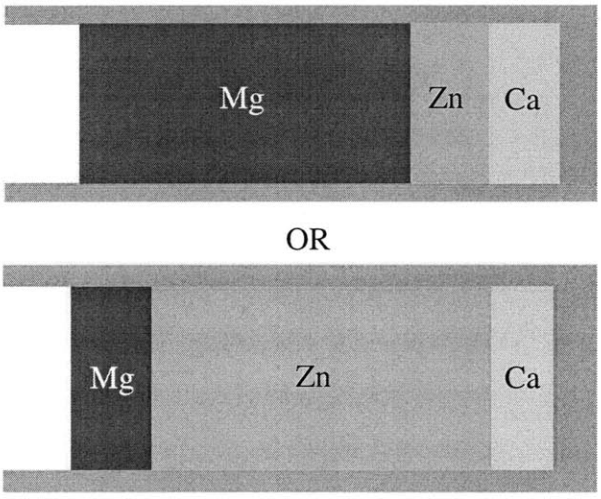

Figure 4.1. Schematic for hypotheses of possible ash plug compositions.

1. The Ca and Zn ash layers may be minimal, and the plug may be almost completely Mg ash, which would be consistent with the prevalent ash distribution/mobility theories.
2. The Mg ash layer may be found to be thin and the majority of the plug may actually consist of Zn ash, as very little Zn was found deposited along the channel walls.

Further investigation is required to confirm or refute the two theories presented above, and this should be the focus of subsequent works.

5 REFERENCES

[1] Majewski, W. Addy, "Diesel Particulate Filter." www.DieselNet.com. 2007.

[2] Athanasios G. Konstandopoulos, Margaritis Kostoglou, Paraskevi Housiada, Nickolas Vlachos and Dimitrios Zarvalis (2003) "Multichannel Simulation of Soot Oxidation Diesel Particulate Filters." SAE Tech. Paper No. 2003-01-0839.

[3] Gaiser, Gerd (2004) "Prediction of Pressure Drop in Diesel Particulate Filters Considering Ash Deposit and Partial Regenerations." SAE Tech. Paper No. 2004-01-0158

[4] Sappok, Alexander. "The Nature of Lubricant-Derived Ash-Related Emissions and Their Impact on Diesel Aftertreatment System Performance." Massachusetts Institute of Technology Doctoral Thesis. 2009

6 APPENDIX

Preparing Sample

Contact: Yinlin Xie (xieyl@mit.edu)

For putting sample in epoxy

- Line cup with non-stick gel
- Place samples vertically in crucibles
- Use designated "resin" and "hardener" measuring beakers to measure 15 parts resin to 2 parts hardener by volume (45 part resin to 6 hardener for 2 samples)
- Mix for about 2 minutes (in a disposable cup)
    - Slower mixing will create less air bubbles
- Place crucibles in chemical fume hood
- Pour epoxy very slowly into cups
- Leave "do not touch" note with name and email

Grinding procedure

- Take samples out of crucibles
- Use sanding disc at the end of the row without sample holders
    - Grind a chamfer onto sample face edges
    - Grind down bottom face (if the edge is curved)
    - Make sure water on the machine is running
    - Rinse sample
- Set up the six sample holder – make sure everything is clean (can use tap water)
- Insert sand paper on plate and insert disc ring and guard
- Lower holder and lock it into place in lower left corner
- Insert samples into holder in an even pattern around center
- Set machine settings (see below)
- Turn machine water on
- Start machine
- Rinse samples immediately
- Rinse holder, ring, and plate
- Throw away sand paper
- Insert next paper (see below)
- Repeat for all different grits of sand paper

Polishing procedure

- Blow dray samples and holder
- Get 0.3 μm Al_2O_3 disc
- Place disc on beaker or holder in sink
    - Get cotton swab from either drawer or cabinet
    - Rinse with de-ionized water and cotton swab
- Put plate in machine

    - Insert guard
    - Set machine (see below)
    - Squirt disc with white solution (in nozzled bottles with "0.3 μm Al_2O_3" label)
    - Lower holder and insert samples
    - Squirt solution onto disc and samples about every 10-15 seconds
    - Rinse samples immediately with de-ionized H_2O
    - Rinse plate with de-ionized H_2O and cotton swabs
- Place plate back in box
- Clean everything
- Fill a random beaker and rinse out drain

SEM Procedure (JEOL 5910)

Contact: Patrick Boisvert (pboisver@mit.edu)

- Press "Vent" button
- Scrape tape off bottom if necessary
- Place tape from edge of DPF on top of the sample to the opposite edge underneath the sample
- Place sample onto medium sized tray with no plate
- Measure height from top of tray to top of sample
- Use pronged tool to place into SEM (push until it clicks)
- Open SEM control program
    - Click "Number" or "Note" on bottom of window
        - Click "Auto Function"
        - Change specimen height to measure sample height
- Click "Evac" button
- Wait until appropriate pressure (needle should match drawn in arrow)
- Put SEM on "Scan 2"
- Set "Acc. Volt" to 15 kV
- Adjust Z until desired distance from sample
    - Working Distance should be about 9-10 mm
    - Focus accordingly (first Coarse mode and then Fine)
- Open "Esprit" program
    - Open "Objects" tab for elemental imaging and run analysis
- Enter session info into log form on computer

Linked References (not printed)

1 Majewski, W. Addy, "Diesel Particulate Filter." www.DieselNet.com. 2007.

2 Athanasios G. Konstandopoulos, Margaritis Kostoglou, Paraskevi Housiada, Nickolas Vlachos and Dimitrios Zarvalis (2003) "Multichannel Simulation of Soot Oxidation Diesel Particulate Filters." SAE Tech. Paper No. 2003-01-0839.

3 Gaiser, Gerd (2004) "Prediction of Pressure Drop in Diesel Particulate Filters Considering Ash Deposit and Partial Regenerations." SAE Tech. Paper No. 2004-01-0158.

4 Sappok, Alexander. "The Nature of Lubricant-Derived Ash-Related Emissions and Their Impact on Diesel Aftertreatment System Performance." Massachusetts Institute of Technology Doctoral Thesis. 2009